Rijksuniversiteit Groningen

Master's thesis

Production and transmission of ions in the CISe setup

Author
L. Blaauw

First Supervisor
Prof. Dr. J. Even

Second Supervisor
Prof. Dr S. Hoekstra

Abstract

Gas catchers are widely used for slowing down energetic ions in order to prepare them for precision mass measurements. Impurities in the gas can affect the extraction efficiency from the gas catcher. However, CISe aims to make use of this effect and explore the potential of chemical reactions inside a gas catcher by investigating chemical isobaric separation (CISe) techniques. The aim is to use this technique to measure the mass of ^{100}Sn with high precision. ^{100}Sn can be produced by a fusion evaporation reaction that also produces a large amount of unwanted isobaric by-products such as ^{100}Ag, ^{100}Cd and ^{100}In. When mass measurements on ^{100}Sn are to be performed, it needs to be separated from these by-products. In order to develop a suited chemical system, a gas catcher is built where stable isotopes of the ions of interest can be produced by laser ablation. The ions can be identified by a qToF mass spectrometer that is coupled to the system. For this thesis, experiments on the production and transmission of the ions are performed and discussed.

October 28, 2021

This thesis was financially supported through NWO-natuurkunde Projectruimte grant (project number: 680-91-103).

Contents

1 Introduction

In the framework of this thesis, experiments on the creation and the guiding of ions of stable isotopes of silver, cadmium, indium and tin (proton number 47-50) inside the CISe setup are performed and described. CISe stands for Chemical Isobaric Separation. This project aims to separate nuclides that have different amount of protons, but the same number of nucleons (isobars) and therefore similar mass, with the help of chemical reactions. This is done inside a gas catcher with 50 mbar of helium and a reactive gas. The to be investigated species are present as ions and are created by means of laser ablation. These ions will be slowed down by the helium and will or will not react with the reactive gas. When the reaction happens, ionic molecules are formed which have a larger mass than the initial, atomic ions. If the reactive gas reacts with one element, but not with another, the two can be separated in a quadrupole mass spectrometer because of their mass difference. The goal is to find a reactive gas that does not react with the element of interest, but does react with its isobars or the other way around. The ion of interest can than be separated from its isobars and can be detected by an MCP (microchannel plate) detector in the qToF (quadrupole time of flight) mass spectrometer where its mass to charge ratio can be displayed.
Before being able to investigate the chemical reactions in the gas catcher, the efficiency of the CISe setup needs to be optimized. The aim is to guide as many of the created ions as possible to the detector such that it results in the largest possible ion transmission rate. The guiding is done with techniques like electric field gradients, RF ion guidance over a surface and linear RF ion guiding using hexapoles. The efficiency of different parts in the setup are investigated by measuring the charges of ions as a current and using electro-optical simulations performed with the SIMION [1] software.

1.1 Motivation

The goal for this project is to apply the technique of CISe for accurate mass measurements of ^{100}Sn. These are of use for the investigation of the rapid proton capture process (rp-process.) This is the process where nuclei in high-temperature and hydrogen-rich environments, such as the core collapse of a supernova, perform consecutive proton captures to create proton rich nuclei. It is one of the processes responsible for the formation of elements heavier than iron. An image of, a close-up of, the nuclear chart on which the predicted path of the rp-process is indicated is given in Figure 1.1. In this figure the mass accuracy of the isotopes [2] [3] is indicated. The path of the rp-process indicated in Figure 1.1, shows that the mass accuracy of most isotopes on and around this path have an error of more than 60 keV. Many of them are never measured directly, but their mass is extrapolated from their decay type and the measured masses from other isotopes that it might decay to. Knowing the masses of these nuclides is very important for improving the prediction of the path of the rp-process, since from the mass, the nuclear binding energy of the nuclides can be determined. It is equivalent to the mass defect: the difference between the mass of the nuclide and the mass of the constituent protons and neutrons if they would have been free and not bound to a nucleus. This is given by the Einstein formula $E = mc^2$ where E is the binding energy and m is the mass defect. The proton capture cross section for these nuclides can be determined and from the masses, Q-values for beta decays can be extracted, providing a better understanding in the forming and decay of the particles involved in the rp-process.

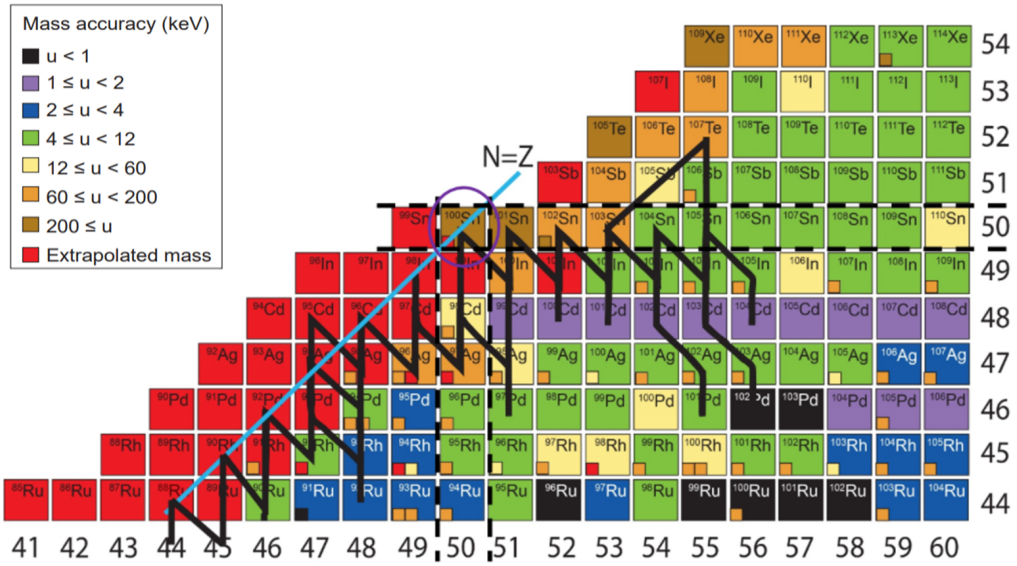

Figure 1.1: *Close up of the nuclear chart around the end point of the rp-process. The black line indicates the path of the rp-process. The blue line indicates the N=Z nuclei. The colour code corresponds to the uncertainty of the measured masses. The dashed lines indicate the N=50 and the Z=50 nuclei.*

^{100}Sn is such a nuclide for which the mass is not very accurately known. It can be created in a fusion evaporation reaction where a ^{50}Cr beam is accelerated to 255 MeV onto a ^{58}Ni target: ^{58}Ni (^{50}Cr, α4n) ^{100}Sn. This reaction is very favourable for the creation of nuclei around ^{100}Sn [4]. So, during this reaction, not only ^{100}Sn is created, but also unwanted by-products. Among them are isobars of ^{100}Sn: ^{100}Ag, ^{100}Cd and ^{100}In. They have similar mass and additionally have also higher production cross sections for this reaction than ^{100}Sn. Here is where CISe is of use. In CISe is investigated how Sn can be separated from Ag, Cd and In. At the same time, it can also be used for the separation of one of either Ag, Cd and In from their isobars to perform mass measurements on them. Knowing their q-values is also very important since these elements are also involved in the rp-process.
In order to investigate this systematically and have enough ions for good data, ions of stable isotopes of the four metals, Ag, Cd, In and Sn, are created by laser ablation. Under the influence of a pulsed laser beam, many more ions per second can be created than during the nuclear reaction. Ablating the metal targets creates only stable ions, which is more efficient for investigating than radioactive ions that are created during the nuclear reaction. For example, ^{100}Sn has a half life of approximately 1.1 seconds [5]. Also, having ions of only one element at a time makes it easier to investigate their properties.

2 Laser ablation

Laser ablation can be described as "explosive laser-material interaction" [6]. It is the process of removing material from a solid surface by heating the target using laser pulses. Laser ablation has many applications, for example laser cleaning [7], laser drilling [8] and LASIK (laser eye surgery [9],) but in experimental physics, it is mainly used for chemical analysis of the removed particles. This is also what is done in the CISe experiment. Sample material is removed in the form of plasma, which consists of neutral atoms or molecules that were present in the sample, ions of these atoms/molecules and free electrons. The ions can have a charge of +1 or +2 and the amount of electrons that are generated will be equal to the charge of the ions combined. The ions can then be analysed by mass spectroscopy. Benefits of laser ablation include no sample preparation or sample size requirements: laser pulses can ablate any solid target surface, there is no waste and there is no need for a high vacuum, because of the highly local heating of the target surface. Since the laser beam is focused on the spot on the target, the gas surrounding the target will not receive as much heat as the target surface. This is beneficial for ion creation inside a gas chamber. A sketch describing laser ablation is given in Figure 2.1.

The way the surface is heated, and therefore the amount of ions created (ablation rate,) will depend on the laser flux (laser power per area,) laser wavelength and pulse duration. These parameters will also not have the same effect on different target materials. The ablation rate depends on the optical properties of the material (Ionization energy, melting point, heat conductance.) Therefore, it is not immediately clear what the threshold for the flux and pulse duration will be in order to have the minimal amount of material ablated (ablation threshold.) It can be estimated that below a flux of 10^6 W/cm^2 with pulses of the order of microseconds or longer the dominant process for material removal is vaporization. The laser-material interaction is highly thermal and melting of the target surface is common. No ion containing plasma is generated. Above 10^9 W/cm^2 with pulses of the order of nanoseconds or shorter, the dominant process will be ablation. Here, the transport of the energy through the vaporization on the surface takes longer than the duration of the laser pulse. The fact that the energy is not conducted very deep into the target material, the laser pulse leads to a local increase of energy right underneath the surface where the material will reach its vaporization temperature before the surface layer can vaporize. Temperature and pressure at the vapor are raised to such an extent that it will cause the surface to explode and release the atoms, ions and electrons that were created at the vapor due to the energy of the laser pulse. Because of this, it is also expected that a material with a better heat conductance has a higher ablation threshold. Melting of material does often not occur during ablation, although, that also depends on the wavelength [10].

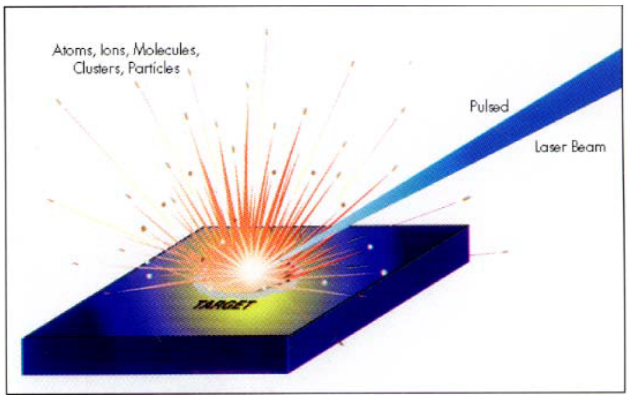

Figure 2.1: *Sketch describing particle creation by laser ablation according to [6]*

A long wavelength (infrared) will mainly induce thermal effects, including melting and less ionization. A short wavelength (ultraviolet) will mainly induce photo-chemical effects, breaking chemical bonds of molecules and between atoms and will reach the ionization energy, the energy needed for a photon to remove an electron from the atom, faster. Radiation in between these extremes, including visible light, will cause both thermal and photo-chemical effects, but to what extent depends, as mentioned before, on the optical properties of the material used. For CISe, a wavelength that provokes photo-chemical effects is desired, but reducing all thermal effects is not needed for the creation of ions. Green light with a wavelength of 532 nm is then sufficient. Many ions can be created easily and it is safer in use than invisible ultraviolet radiation.
Since the ablation rate and ablation threshold depend on the optical properties of the ablated material, we can compare the thermal conductivity, melting point and ionization energies of the materials used in CISe: silver, cadmium, indium and tin. These properties are given in Table 1.

Table 1: *Ionization energies, melting point and thermal conductivity of silver, cadmium, indium and tin.*

Element	**1st / 2nd ionization energy (eV)** [11]	**Melting point (K)** [12]	**Thermal conductivity (W/mK)** [13]
Ag	7.5 / 21.5	1234.9	430
Cd	9.0 / 16.9	594.2	96
In	5.8 / 18.9	429.7	82
Sn	7.3 / 14.6	505.1	67

3 Method and setup

The setup for CISe consists of the following parts: a laser table (including laser and optics,) a gas catcher, an ion guide and a qToF mass spectrometer. Ions are created by laser ablation inside the gas catcher, slowed down and guided to the ion guide that leads them to the qToF where their mass to charge ratio is detected. In this section, a description of these parts and their function within the setup is given. In Figure 3.1, a photo of the whole setup is shown.

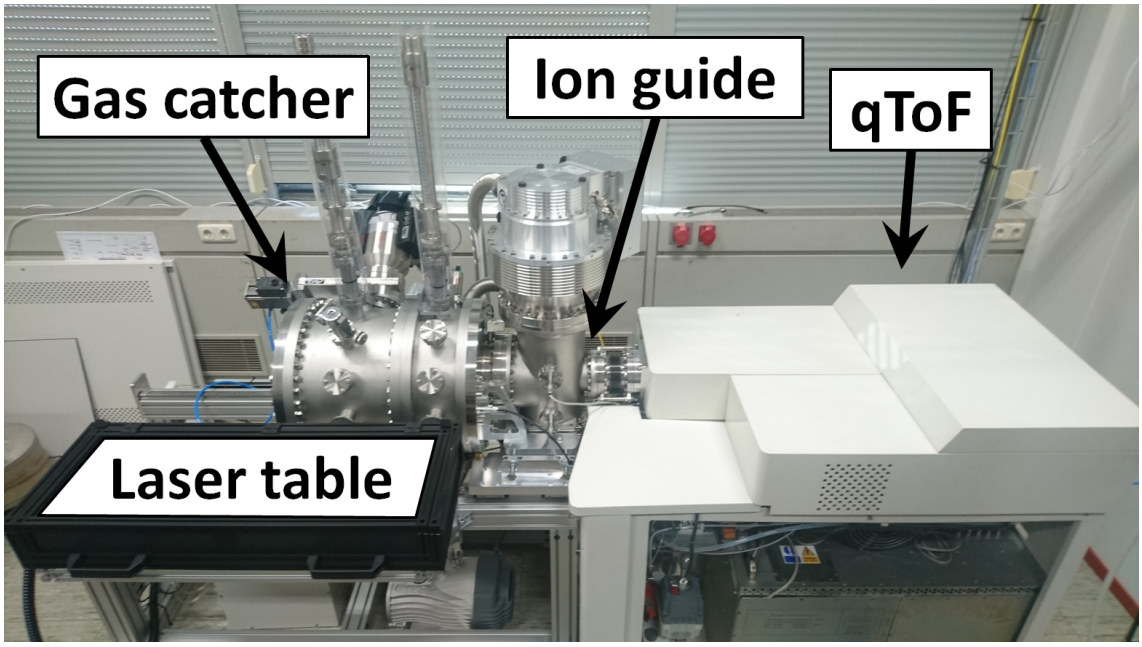

Figure 3.1: *A picture of the CISe setup*

3.1 Laser setup

In order to create ions inside the gas catcher, a laser is needed to perform laser ablation on metal targets. The laser that is used in the setup is the Minilite II [14]. This is an Nd:YAG pulsed laser which can shoot laser pulses of about 5 to 6 nanoseconds at wavelenghts of 1064 nm (infrared,) 532 nm (green) and 266 nm (ultraviolet.) The optical features of the laser are included in the laser head (see Figure 3.2.) The beam is induced by a flash lamp that energizes a rod made out of Nd:YAG crystal creating photons that can be collected and released as a laser beam. The wavelength used for ablation is 532 nm. This wavelength can be chosen by guiding the laser beam, with typical wavelength of 1064 nm, through a crystal that doubles the frequency of the beam to make it travel with the second harmonic of the initial beam: 532 nm. The laser head also has an attenuator on top which can be used to regulate the laser power. The laser beam leaves the box through the hole seen in Figure 3.2 and, in case needed, can be blocked by the lid in front of the hole.

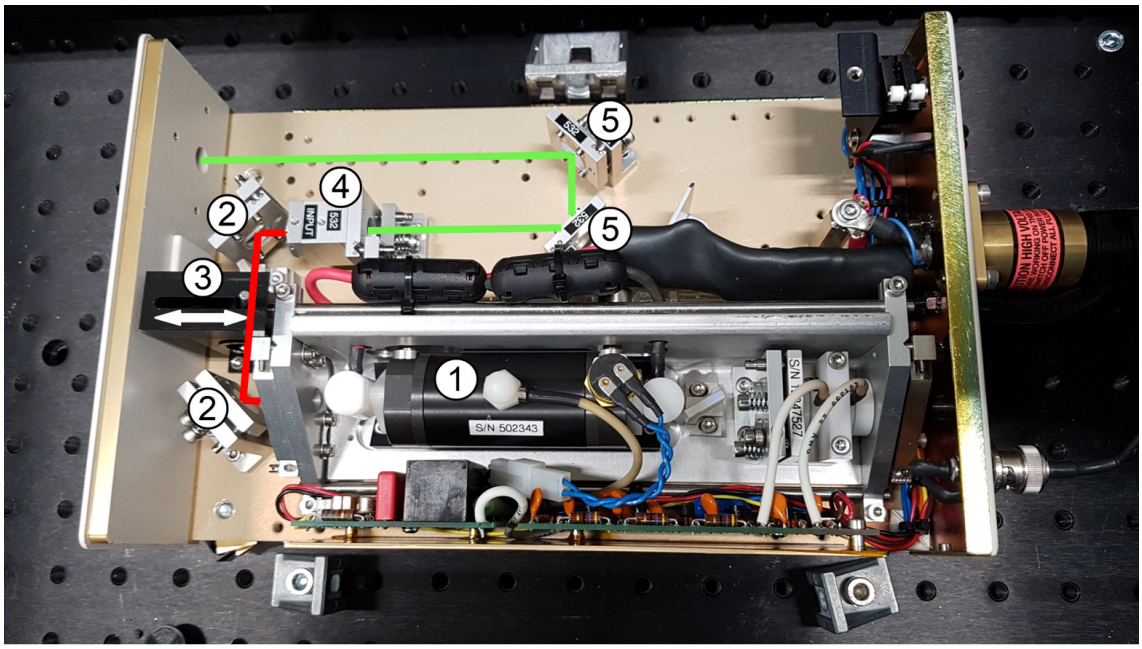

Figure 3.2: *Photo of the laser head with the beam path indicated. The numbers indicated correspond to: 1. flash lamp and Nd:YAG crystal rod to induce the laser beam, 2. 1064 nm reflecting mirrors, 3. attenuator for regulating laser power (push to the left to increase laser power), 4. frequency doubling crystal, 5. 532 nm reflecting mirrors*

After leaving the laser head, the beam is guided to one of the two windows of the gas catcher by optical mirrors and lenses that are placed on a laser table (see Figure 3.3.) The laser beam takes one of two possible paths to reach one of the two target holders inside the gas catcher. These paths are indicated in the figure. The lenses have a focal range of 50 cm such that the beam hits the target right before it reaches its focal point. The laser table is surrounded by a box made of light blocking material such that it is safe to use the laser when the box is closed.

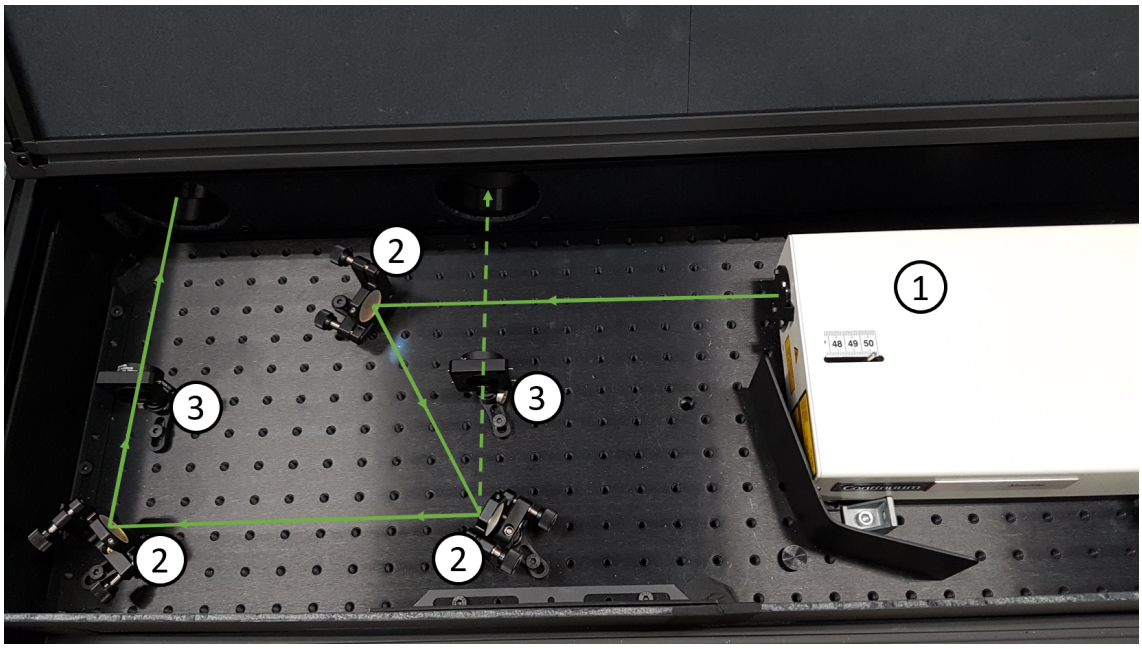

Figure 3.3: *Picture of the laser table. Indicated are 1.laser head, 2.mirrors, 3.lenses and the two possible focal paths of the laser*

3.2 Gas catcher

Inside the gas catcher, ions are created and modified such that they can be guided to the ion guide. A sketch of the gas catcher is given in Figure 3.4a. The pressure in the gas catcher can be displayed by a digital pressure gauge that is not calibrated for helium, but is accurate up until approximately 10^{-2} mbar and an analog pressure gauge that can measure pressures of above 1 mbar. The laser beam comes in through one of the two windows to reach one of the two target holders that are present in the gas catcher. The target holders are called 'target holder #1' and 'target holder #2' and their location in the gas catcher is indicated in Figure 3.4a. Target holder #2 is the closest to the ion guide. These target holders are each holding four different metal plates of about 1.8 cm in length (targets, see Figure 3.4b.) The targets are, from top to bottom, silver (Ag,) indium (In,) cadmium (Cd) and tin (Sn.) The holders are able to move up and down in the gas catcher in order to select which target the laser will hit and hence, which metal will be ablated and from which metal ions are created. The gas catcher is filled with 50 mbar of helium gas which is used to slow down the ions created by laser ablation. According to [15], 50 mbar is sufficient to slow down the energetic ^{100}Sn ions of about 67 MeV that are coming into the gas catcher after being created by the nuclear reaction ^{58}Ni (^{50}Cr, α4n) ^{100}Sn at 255 MeV and then guided to the gas catcher through a window (where it loses some of its energy.) Although it is not known what the ion energy or the relation between laser power and ion energy is after laser ablation, the energy of the ions created by laser ablation is much less than the energy of ions coming from the nuclear reaction, so also these ions are slowed down sufficiently by the 50 mbar of helium. While moving

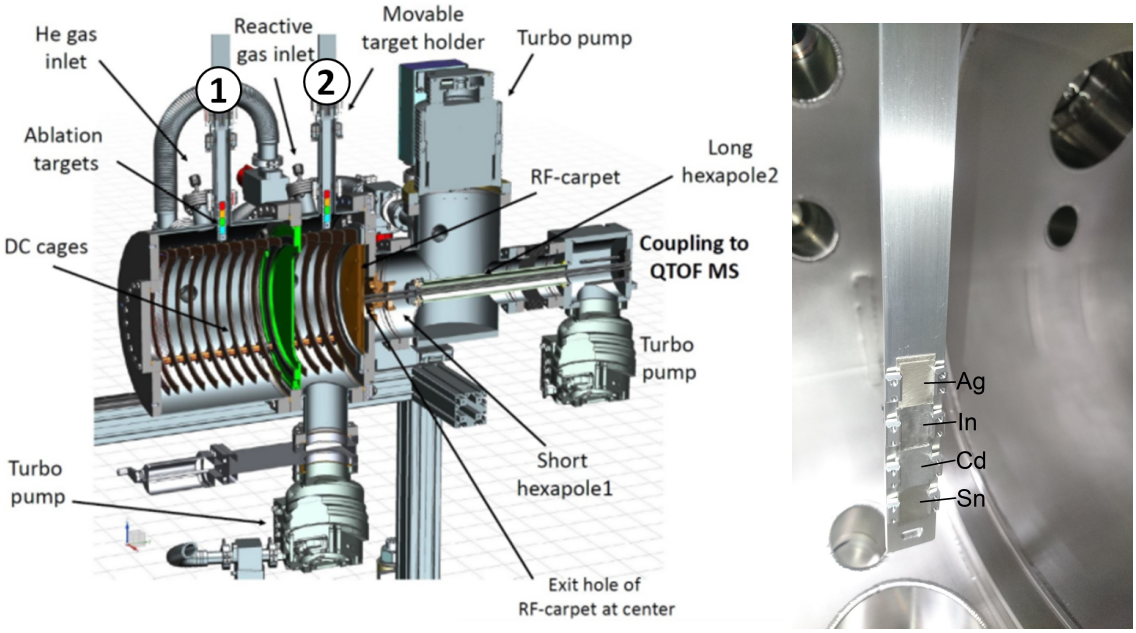

(a) *Schematic picture of the gas catcher and ion guide. The numbers indicate 1. target holder #1 and 2. target holder #2.*

(b) *Target holder with targets*

Figure 3.4: *Images of the gas catcher*

through the gas, the ions will be guided towards the ion guide with the help of an electric field gradient provided by a device called the DC cage. The cage consists of 16 electrode rings with resistors of equal resistance in between them. The first ring has the highest voltage and, due to the resistors, every consecutive ring will have a lower voltage until the last ring, which is the closest to the ion guide, has ground voltage. This goes with equal steps to make the decrease in voltage as gradual as possible. According to Ohm's law, $U = I * R$, the circuit loses a voltage U from one ring to the other due to a resistance R while the current I does not change, leaving the next ring with a lower voltage. Additionally, the first ring (the ring with the highest voltage) has its area filled up with a grid of metal wires. This is to repel the ions and prevent them from flying out of the wrong end of the gas catcher. The gradient will then guide the positive ions from the high voltage region to the low voltage region towards the RF carpet. A sketch of the cage with the electric gradient is given in Figure 3.5. Note: the target holders fit in between the rings of the cage. Target holder #1 is located between the 5th and 6th ring and target holder #2 between the 11th and 12th ring.

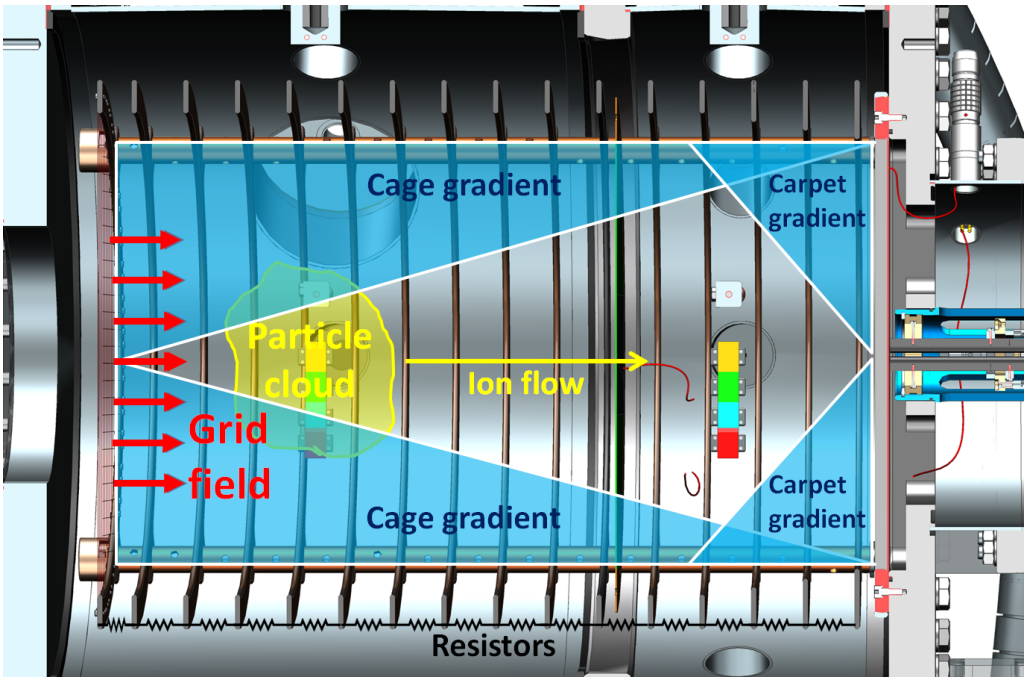

Figure 3.5: *A sketch of the inside of the gas catcher where the electric gradient fields of the cage and the carpet are indicated as well as the field provided by the grid in order to guide ions from the target towards the hole of the carpet.*

3.2.1 RF carpet

Between the gas catcher and the ion guide, there needs to be a pressure difference. The gas catcher needs 50 mbar of helium gas to slow down ions while the ion guide requires the best vacuum possible in order to prevent collisions of ions with the gas during the guidance though the ion guide. To achieve this, there has to be a wall between them, including only a very tiny hole (diameter of 0.45 mm) to let ions go from the gas catcher to the ion guide. This wall is realised as the RF carpet. In order to avoid the ions hitting the carpet when they are guided towards it by the gradient of the cage, the carpet has a series of concentric ring electrodes, which have a phase difference of 180° between adjacent electrodes. That causes every other ring electrode to have a certain positive voltage and the remaining rings to have a negative voltage with the same magnitude. So every ring has the opposite voltage of its adjacent rings. The voltage on every electrode is then alternating between positive and negative with a certain RF frequency. This results in a time-average repelling force on ions away from the carpet's surface. This repelling force together with the force coming from the cage gradient that is pushing the ion towards the carpet, causes the ions to hover right above the surface of the carpet. When only using the RF, the ions will keep hovering over the electrodes in random directions. In order to guide them towards the center of the carpet where the hole is located, a DC gradient is applied. This works according to the same principle as the DC gradient of the cage. The outermost ring has the highest DC voltage offset and this is gradually

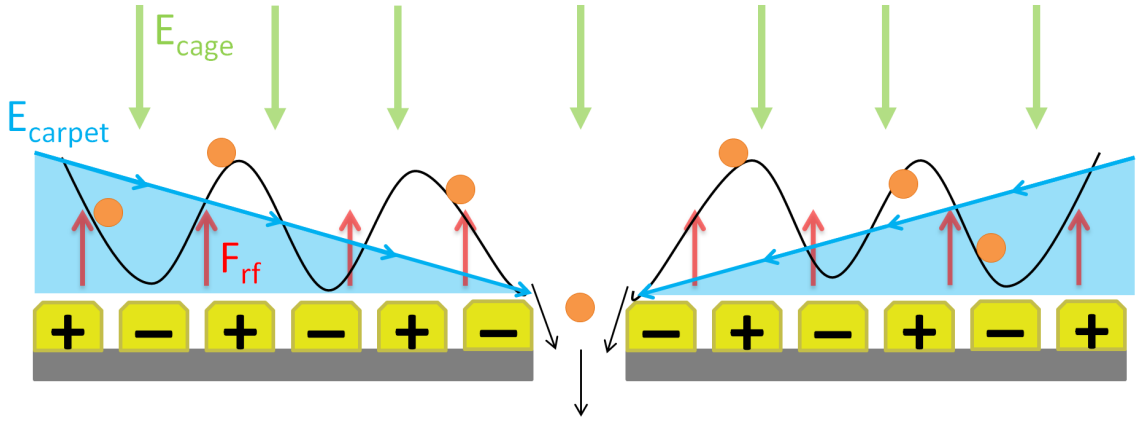

Figure 3.6: *Sketch of the carpet fields and forces on the ions. E_{cage} represents the electric field gradient of the cage that is pushing the ions towards the carpet. E_{carpet} represents the electric field gradient of the carpet that is guiding ions towards the hole. F_{rf} represents the time-average repelling force on the ion by the RF voltage. The orange circles represent the ions and the black lines are their wave-like trajectories when hovering above the surface of the carpet.*

decreasing until the ring in the center has ground voltage. This DC gradient is forcing the ions towards the middle of the carpet to safely pass through the hole where a supersonic gas jet, created by the pressure difference between gas catcher and ion guide, transports them into the ion guide section. The forces that are working on the ions when they approach the carpet is illustrated in Figure 3.6. Note: if there was no RF voltage, but only a DC gradient, ions would still be guided towards the center. However, most of the ions would be collected at the centermost rings and will not reach the ion guide.
A schematic of the carpet is given in Figure 3.7. Just as with the cage, the resistors between the rings provide the DC gradient according to Ohm's law. The RF voltage is added through two channels, one with the uneven rings (the outermost rings and every other ring) and one with the even rings (the remaining rings) causing one ring to have opposite voltage of its adjacent rings. The frequency is provided by capacitors between the rings together with a coil according to the principle of the LC oscillation circuit: $f_0 = \frac{1}{2\pi\sqrt{LC}}$ with f_0 the resonance frequency, L the inductance of the coil and C the capacitance of the whole circuit. The resonance frequency of the carpet is approximately 5 MHz with an RF voltage that can go up to 100 V_{p-p}. This means that the voltage of the ring electrodes alternates between 50 V and -50 V with 5 million times per second.

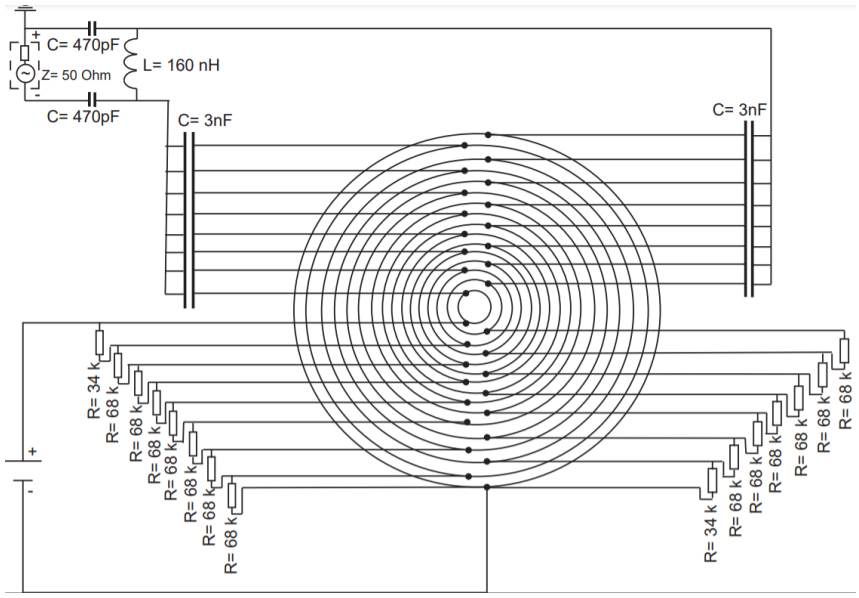

Figure 3.7: *A schematic of the connections in the carpet. The resistors (R) provide the DC gradient of the carpet and the capacitors (C) together with the inductance of the coil (L) provide the RF frequency.*

3.3 Ion guide

This part is used to safely guide the ions to the detector. The ions that are entering the ion guide from the carpet hole feel a force in the direction of the qToF due to a cone shaped supersonic gas jet that forms between the high pressure region (the gas catcher) and the low pressure region (the ion guide.) This gives the ions an energy of roughly 2.8 eV [15] entering the ion guide. In order to confine the ions on a linear axis during the guidance, two hexapoles are used. Hexapoles are multipole ion guides with three pairs of parallel electrode rods that are mostly used for linear ion transport. They have a DC voltage offset acting as an electric potential to the ions as well as an RF voltage applied to the rods. The RF voltage of one rod has opposite sign of its adjacent rods, resulting also in an opposite voltage on its opposing rod. The hexapole has three of these pairs of opposing rods in the configuration seen in Figure 3.8. One rod of such a pair has an electric potential of $\phi = U + Vcos(2\pi ft)$ and the other rod has a potential of $\phi = U - Vcos(2\pi ft)$ where U is the DC voltage and V is the zero-to-peak RF voltage [17]. So, the RF voltage of these rods is alternating between positive and negative with a certain RF frequency f, typically of 1 MHz [18],

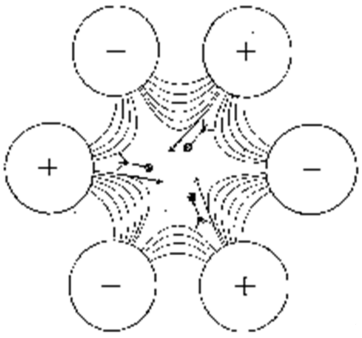

Figure 3.8: *Cross section of a hexapole. Every rod has opposite voltage as their adjacent and opposing rods [16]*

during time t. Every change in potential gives the positively charged ion a pulse in the direction of the negatively charged rod. The next change in potential will result in a pulse in the opposite direction. Due to these constant changes in potential, the ion stays confined around the central axis.[17]. This is illustrated in Figure 3.9 for an initial phase (Figure 3.9a) and a phase of 2π later (Figure 3.9b.) This confines the ions and lead them through the whole hexapole to transmit them.

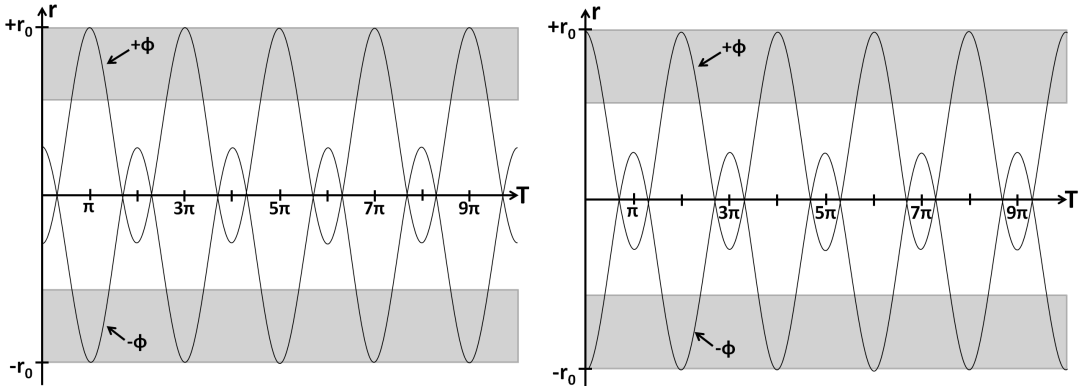

Figure 3.9: *Schematic of the operation of the hexapole ion guide. It shows the electric potential two opposing electrode rods with opposite potential (depicted by the grey rectangles) give to an ion at a certain radial position in the hexapole (r) at a certain phase in time (T) at any point along the length of the hexapole. One of the rods has potential of $+\phi$ and the other one has a potential of $-\phi$.*

The pressure in the region directly behind the carpet is approximately $2 * 10^{-3}$ mbar. In the qToF, the pressure should be at least of the order of 10^{-6} mbar. In order to achieve a more gradual pressure difference between the ion guide and the qToF, we do not use one long hexapole, but instead use one short hexapole in the region directly behind the carpet and a long hexapole to lead the ions into the qToF. In between these two hexapole, three electrical lenses are located, each consecutive one with a smaller diameter. Through differential pumping, the pressure of the region around the second hexapole is then reduced to $5 * 10^{-5}$ mbar, while the pressure around the first hexapole maintains $2 * 10^{-3}$ mbar. When the ions pass the lenses, they will feel an additional gas jet induced by these two pressure regions. In order to gradually guide the ions from one pressure region to another, an electrical gradient is provided by the DC offset voltage of the hexapoles and the lenses. Since the ions are positively charged, this gradient has an increasingly negative voltage; hexapole 2 should have the largest magnitude.

3.4 qToF

The qToF mass spectrometer is the device where ions can be filtered by mass and detected. The most prominent features of this qToF are the quadrupole mass filter that is used for ion selection by mass and the time of flight detection method to determine the mass to charge ratio (m/z) of the ions.
Just like the hexapole, the quadrupole is a multipole ion guide. They have two pairs of electrode rods and the main difference with the hexapole is that in the quadrupole, opposing rods have the same potential instead of opposite potential. Due to this, the ions are alternately focused in the horizontal plane and the vertical plane to create a three-dimensional wave. This configuration and the combination of the DC and RF voltages make it possible to operate the quadrupole as a mass filter [19]. A certain m/z can be selected and then only ions with that m/z will reach the end of the quadrupole and get transmitted. The others will have unstable trajectories and will collide with the rods.
The motion of ions with low m/z is dominated by the alternating RF voltage. For every change in rod potential, the ions receive an additional energy increasing the amplitude of their wave-like motion. If this amplitude gets large enough, the ions collide with a rod and will therefore not be transmitted by the quadrupole. Since lower masses have larger acceleration rate, they are more sensitive to the change in potential of the rods and therefore, a low m/z cutoff can be set by changing the RF potential or the RF frequency. Then only ions with a higher m/z than this cutoff will be transmitted.
The quadrupole also has a high m/z cutoff. This is because of the DC voltage. Since low m/z respond very quickly to the potential change of the rods, they are refocused with every polarity change. Therefore, the DC potential does not affect these ions. This is not the case for high m/z ions. Under the influence of the DC voltage, they will slowly drift away from the central axis of the quadrupole such that they do not reach the detector.
The quadrupole can thus act as a low m/z and high m/z filter by setting certain values for the DC and RF potentials such that only a certain m/z range of ions can be transmitted by the quadrupole or even a single m/z value.

Ions that pass the quadrupole are guided towards a microchannel plate (MCP) detector where their m/z is detected according to the Time of Flight (ToF) method. This method is based on the fact that monoenergetic ions with a different m/z have different velocities and thus take different times to travel a certain distance. A packet of ions that is ejected out of the quadrupole receives an electric field pulse that gives the ions energy. Ions with different m/z will gain different velocities and will arrive at the MCP detector at different moments. The time between the electric field pulse and the arrival at the MCP detector is recorded and subsequently, a m/z is calculated. In this way, the ions can be distinquished by their mass to charge ratio.

4 Measurements and results

In this chapter, measurements on the transport of the ions in the setup are described and their results are shown and discussed. In the gas catcher, ions are created by laser ablation, slowed down by the helium gas and transported via the ion guide to the detector. To gain a better understanding of the guidance of ions, the ion transport has been studied in steps. First it is checked if particles are created, after that it is investigated if and how many ions reach the carpet and lastly, the transport through the ion guide will be examined.

4.1 Current measurements

In order to check if ions are created and whether they reach the carpet, measurements of the current is done on various components in the setup (see Figure 4.1.) The target holders (number 1. and 2. in Figure 4.1) can measure the current induced by the laser pulses. The charge generated on the target by electrons that have escaped the target is balanced by a return current coming from the ground to neutralize the target [20]. Since for every escaped electron, a negative charge is taken from an atom, thus creating ions, the measured current can give us an indication of the amount of ions that are created.
The carpet (number 4. in Figure 4.1) and the lenses (number 5. in Figure 4.1) can be used as a Faraday cup. A Faraday cup is a device that detects current from a beam of ions. It is made out of conducting material that can register the charge of an ion whenever it hits the device [21]. This particle then loses its charge and sends it to the Faraday cup. This charge can be measured as a DC current. The carpet and lenses can be considered Faraday cups since the electrical gradient of the cage separates the positively charged ions from the negatively charged electrons and therefore we can assume that all charges detected on the carpet or lenses come from the stream of ions. This gives us an indication of the amount of ions that are reaching these parts of the setup.
It is also possible to measure a current on the cage (number 3. in Figure 4.1.) However, this cannot be a good indication of the amount of ions created, since it is unclear whether the measured charges come from ions or electrons. It is more likely that electrons hit the cage, since the cage is positively charged and might attract the electrons, but it is not impossible for the energetic ions to break the potential barrier and hit a ring of the cage. The current is measured with a multimeter (Keithley model DMM7510) that has an accuracy of 0.1 pA (which correspond to $6.241 * 10^6$ elementary charges) with fluctuations of $\pm$ 100 pA. The connections for the current measurements are drawn in Figure 4.2. The multimeter and the device are connected via a connection box in order to provide a voltage to the device from a power supply simultaneously with measuring the current on the device coming from the charged particles. In order to let the carpet function as a good Faraday cup, a slight modification had to be done: the resistors needed to be eliminated by adding a layer of soldering material over all the resistor connections. Now, the circuit shown in Figure 3.7 is fully conducting, allowing all charges to be measured by the multimeter.

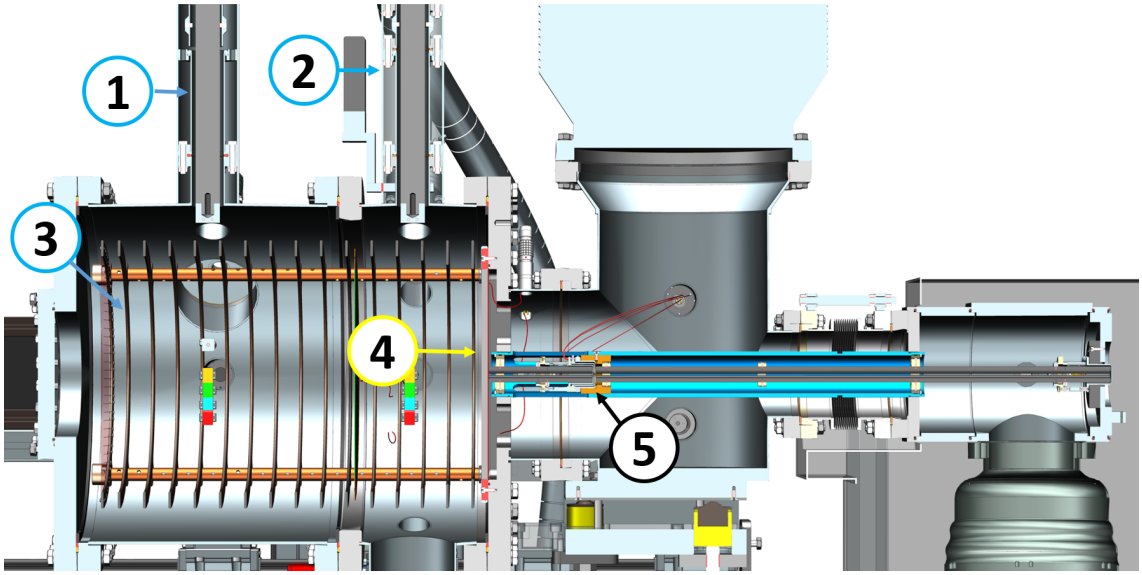

Figure 4.1: *Cross section of the gas catcher and ion guide. Indicated are the components where a current can be measured: 1. target holder #1, 2. target holder #2, 3. cage, 4. carpet, 5. lenses. Only 4 and 5 act like a Faraday cup.*

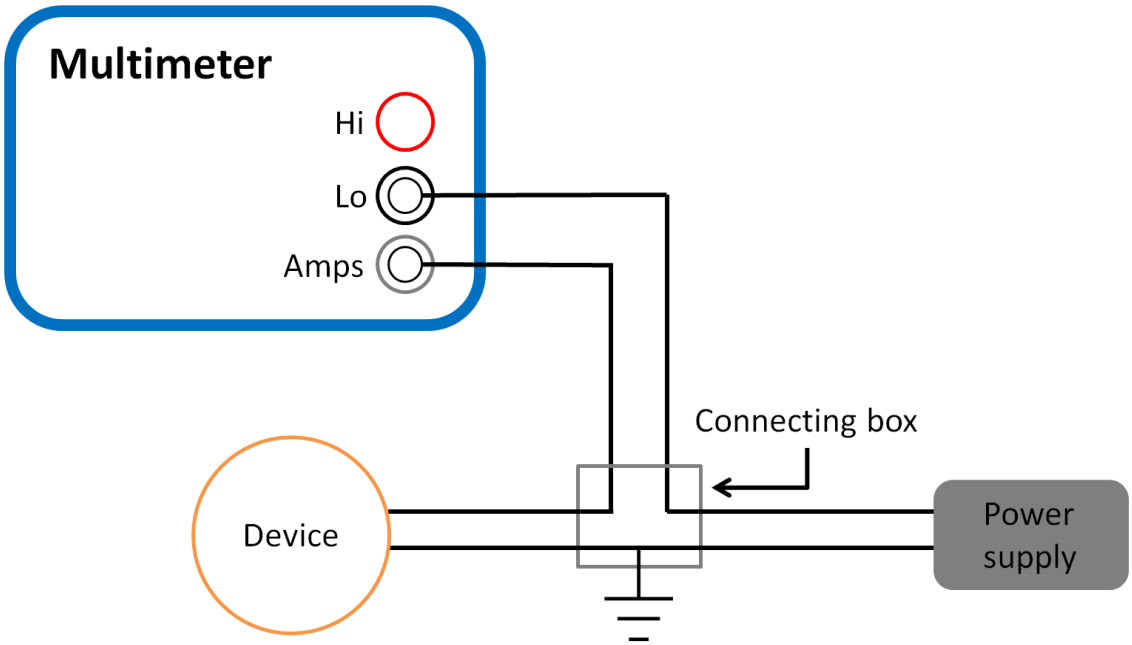

Figure 4.2: *Schematic of the setup to measure the current that is provided by ion charges on a device while simultaneously providing a voltage to the device.*

4.1.1 Creating ions

Measurements of the induced current on a target holder show that ions are indeed created by ablation inside the gas catcher. Table 2 shows the current detected on target holder #2 (number 2. in Figure 4.1) for different laser powers when ablating the four different targets. Each measurement is done for 10 minutes and the average current over this time span is recorded. For every measurement, a fresh, initially non-ablated spot on the target is used and the angle of the laser beam on the target is also kept constant. For these measurements, the pressure used for these measurements is relatively low and not very accurately known, since the digital pressure gauge is not calibrated for helium and the analog pressure gauge cannot recognise these low pressures. We estimate that the pressure is in between $1 * 10^{-2}$ mbar and $5 * 10^{-1}$ mbar. The current on the target holder for a higher pressure of 50 mbar is given in Table 3. For all of these measurements, no RF voltage was applied to the carpet, such that this could not influence the current measured, hence similar results should be found for target holder #1 (number 1. in Figure 4.1.)

Table 2: *Average current measured over 10 minutes on target holder #2 for different laser powers and every target on a pressure of about 0.1 mbar. The current on cadmium, indium and tin for laser power 171.2 mW is not measured.*

pressure 0.1 mbar	Average current (± 0.1000 nA)			
Laser power (± 1.5 mW)	Cadmium	Indium	Silver	Tin
5.1	0	0	0	0
9.2	0	0	0	0
16.7	0	0.0144	0	0.0257
26.6	0.0355	0.3986	0	0.0373
38.8	2.1969	1.4266	0	0.8848
51.0	4.5515	1.9006	0	1.7519
67.2	8.7753	2.7070	0.0239	3.8528
80.2	23.4110	4.6056	0.0741	5.7323
108.4	71.6780	14.1215	0.2267	9.7825
126.9	188.0563	40.6232	1.0308	50.8370
145.8	339.4889	84.4301	9.3365	82.3736
171.2	/	/	40.0878	/

The results in tables 2 and 3 show that for a higher laser power more ions are created. Taking the assumption that the induced current corresponds to all electrons that escaped the target and only ions with a single elementary charge are created, then the amount of particles created for, for example, cadmium is $2.22 * 10^8$ (0.0355 nA) for a laser power of 26.6 mW and $2.12 * 10^{12}$ (339.4889 nA) for a laser power of 145.8 mW.
Moreover, it can be concluded that the different target materials have different ablation behaviour. For example, the laser power at which a current is first detected is much higher for silver than for the other materials; For indium and tin, a current is detected at 16.7 mW and for silver a current is measured for laser powers above 67.2 mW indicating that silver has a higher ablation threshold. From Table 2 can be concluded that indium and tin have similar ablation behaviour. A current is measured on relatively low laser power and for each value of laser power, their current

Table 3: *Average current measured over 10 minutes on target holder #2 for different laser powers and every target on a pressure of about 50 mbar.*

pressure 50 mbar	Average current (± 0.1 nA)			
Laser power (± 1.5 mW)	Cadmium	Indium	Silver	Tin
67.2	2.0446	0.1017	0	0.1764
80.2	8.0965	1.9445	0.1534	0.3982
108.4	17.0702	2.4371	0.1812	1.7336
126.9	27.1018	6.5964	0.561	3.7551

measured is comparable. This can well be seen in Figure 4.3 where the current measured on the carpet over time for the different materials is shown (the pressure here was around 50 mbar.) The ion production of tin and indium has a very high peak in the beginning of each measurement (see Figures 4.3b and 4.3d.) After that peak, it stays constant on a very low (relative to the peak) current. In contrast, it looks like cadmium has a more constant ablation behaviour. The ablation pattern (graph 4.3a) shows a minimum instead of a peak before getting to a constant current. This constant current is equally as high as the initial current measured. The ablation of silver (see Figure 4.3c) is also constant over time, but requires a relatively high laser power to be ablated.

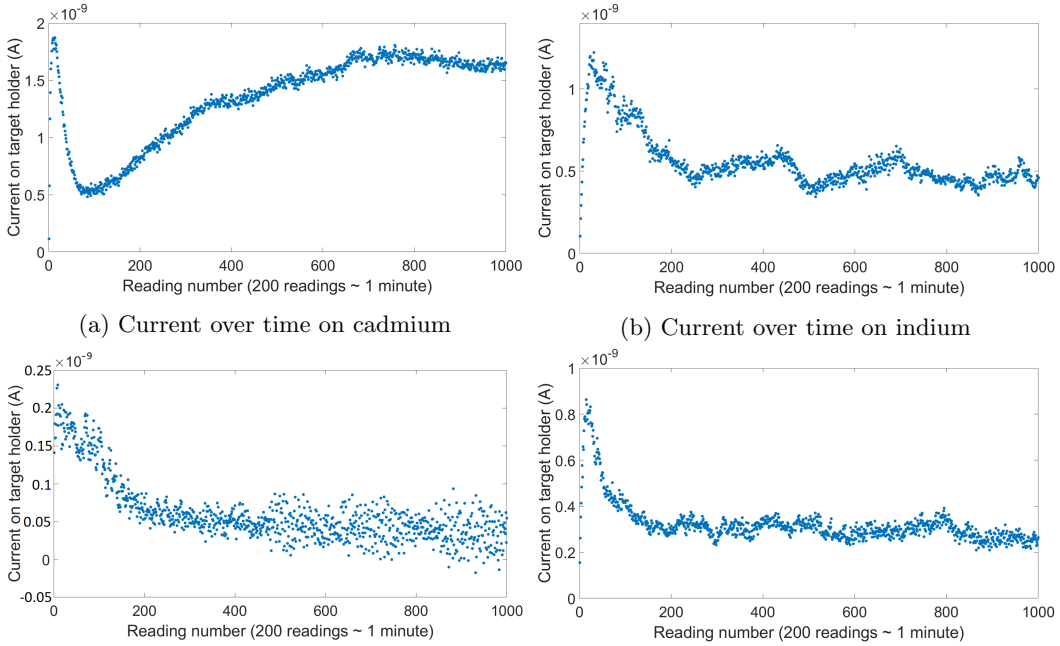

(a) Current over time on cadmium

(b) Current over time on indium

(c) Current over time on silver

(d) Current over time on tin

Figure 4.3: *Current measured on the carpet over time for the four different materials. They show the ablation behaviour of the materials.*

These findings are in agreement with the optical properties of the materials listed in Table 1. Silver is the element with, clearly, the highest melting point and the best thermal conductivity. Therefore, the heat from the laser pulse is well distributed over the material and so, the increase in temperature is not localized resulting in a higher ablation threshold for the laser flux. Tin and indium have the lowest melting point and thermal conductivity and they have, as expected, the lowest ablation threshold. We do not notice a relation between ablation rate and ionization energy. Comparing Tables 2 and 3 we notice that for a higher pressure, the current measured on the target holder is lower. For cadmium this is about 4 times lower and for indium and tin even more than 10 times lower. This means we should have more losses already right after ablation for a higher pressure. That could be caused by the forming of clusters of atoms which consist for the most part out of neutral atoms. So instead of releasing ions and electrons, neutral atoms leave the target. Less electrons leaving the target results in a lower detected current.

4.1.2 Guiding ions to the carpet

In order to investigate if the created ions are guided towards the carpet and how that depends on the parameters pressure, laser power, the electrical gradient of the cage (U_{cage}) and the target holder voltage (U_{th1},) measurements of the current induced in the carpet (number 4. in Figure 4.1) by the ions are conducted. During these measurements, the carpet has no RF nor DC voltage such that these do not affect the ions so ions are collected across the whole area of the carpet.
Most important for the guidance inside the gas catcher is the electrical gradient provided by the cage. For an ideal gradient, ions are guided without any losses from the creation spot to the carpet. Having the right voltage on the target holder that is lowered into the gas catcher and on which the targets are ablated, helps reduce the losses. To investigate the dependence of U_{th1} on the ion guidance, the current on the carpet is measured when ablating cadmium while keeping $U_{cage} = 200$ V and the laser power around 80 mW. Additionally, the current on the target holder for the same U_{th1} values is also measured. For these measurements, target holder #1 is used (number 1. in Figure 4.1.) This one is the furthest away from the carpet, giving a better representation of the guidance than target holder #2 (number 2. in Figure 4.1) since the initial plasma cloud cannot reach the carpet from there.

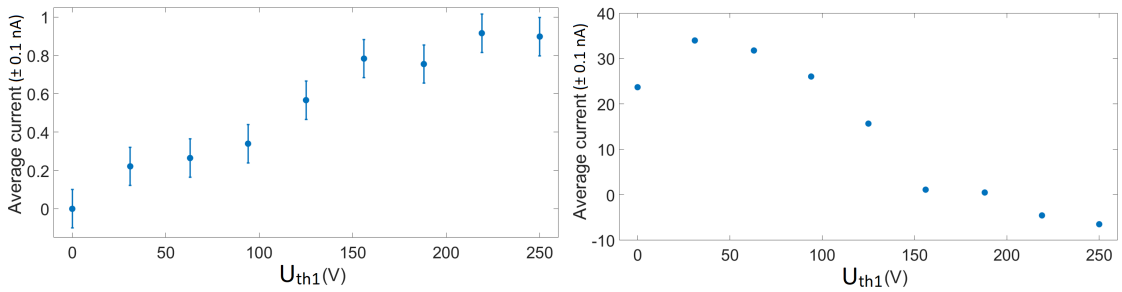

(a) *Average current on the carpet*

(b) *Average current on target holder #1*

Figure 4.4: *Average current (over 5 minutes) measured on the carpet and target holder #1 while ablating cadmium on target holder #1 for different* U_{th1}.

The results are given in Figure 4.4. Expected was to see a peak of current in the carpet for a target holder voltage that is in between the voltage of the neighbouring rings of the cage. For target holder #1 the voltages of these rings are 146.7 V and 160 V. Figure 4.4a just shows that the current on the carpet increases when U_{th1} is increased. Figure 4.4b shows that around these voltages the current measured on the target holder is around zero and for higher voltages, the current even becomes negative. This can indicate that the target holder might pick up charges from the positive ions. This seems a strange conclusion, since a larger positive voltage should repel the positively charged ions. On top of that, Figure 4.4a does not show relatively large losses at these voltages. To make an improvement on these measurement in the future, it could be a good idea to measure the current on the target holder and the carpet simultaneously instead of measuring them separately. In this way they can be compared better to each other. For further measurements it is decided to use a U_{th1} that is 80% of U_{cage}.

The amount of ions that are guided towards the carpet also depends on U_{cage}. For this experiment, the carpet is used as a Faraday cup and it is investigated how many cadmium ions coming from target holder #1 (number 1. in Figure 4.1) hit the carpet (number 4. in Figure 4.1.) This is done for different U_{cage} while U_{th1} is 80% of that of the cage and the laser power is about 190 mW. A larger laser power than in the U_{th1} measurements is chosen here in order to create more particles and therefore detect larger currents to achieve a clearer difference between the measurements.

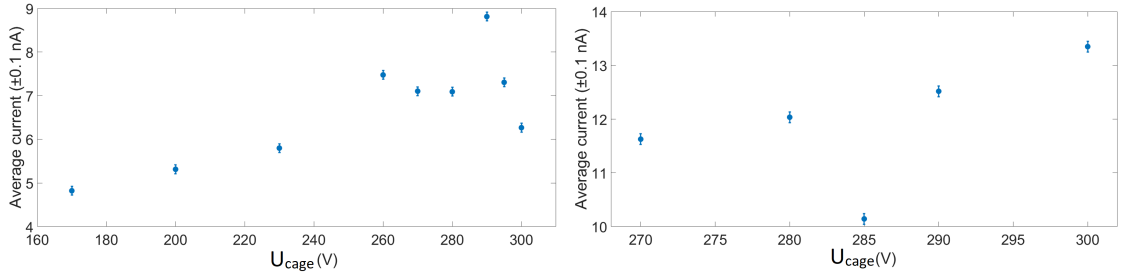

(a) *First measurements* (b) *Retaken measurements between 270V and 300V*

Figure 4.5: *Current detected on the carpet for different DC voltages of the cage.*

The results are given in Figure 4.5, firstly for a U_{cage} range of 170 V to 300 V (Figure 4.5a) and after that, the measurements between 270 V and 300 V were retaken (Figure 4.5b.) This shows what looks like a saturation pattern: the measured current stops increasing after 260 V with only a peak at 290 V. However, in the retaken measurements, there is no peak at 290V nor a saturation pattern. Instead, the current seem to increase with increasing U_{cage}. The measured current is also much higher than in the first measurements. The reason for this is that for the retaken measurements, the laser beam was moved a little bit to the side to reach a fresh spot on the target. This caused a change of the angle the beam makes with the surface of the target, apparently leading to a better ablation. Nevertheless, from these results, the assumption can be made that for a higher U_{cage} more ions are guided to the carpet, at least until a voltage of 300 V. It was expected that for a certain U_{cage}, the current on the carpet does not increase anymore for increasing U_{cage} and hence, reaching a saturation point, making that U_{cage} the optimum voltage for the guidance of ions inside the gas catcher. For now, $U_{cage} = 300$ V can be taken, which is the highest voltage

included in these measurements, as the best ion guiding voltage. However, it is not immediately true that a higher U_{cage} is better for guiding ions through the carpet hole, since in order to get ions through there, the RF of the carpet needs to keep the ions from hitting the carpet. Ions with a kinetic energy that is high enough to break the potential barrier provided by the time averaged RF force pointing away from the carpet will then hit the carpet and are lost. This is not investigated during this thesis.

Using the voltages obtained in the previous measurements (U_{cage} = 300 V and U_{th1} = 0.8*U_{cage} = 240 V) we can investigate the current on the carpet for different laser powers. These following measurements were done on all four target materials, on target holder #1. The pressure in the gas catcher was 50 ± 10 mbar. The average current detected on the carpet over 5 minutes as well as the maximum current reached in the same measurement is measured and depicted in the graphs seen in Figure 4.6 and Figure 4.7 respectively.
As the results in Tables 2 and 3 already showed, the amount of ions increases for higher laser power. A larger current is thus detected for higher laser power on both the carpet and the target holder. Detection of silver starts at a higher laser power than for the other three targets. Moreover, the maximum current for indium and tin is much larger than their average current. Also, the average current for cadmium is larger than for the other targets. These observations are all in agreement with the graphs in Figure 4.3

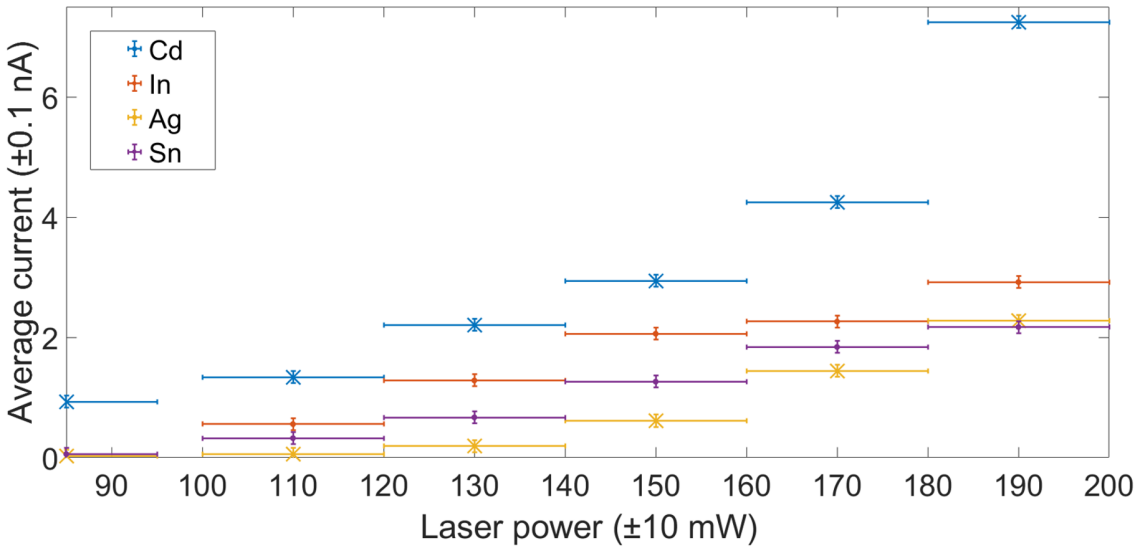

Figure 4.6: *Average current on the carpet measured over 5 minutes for the four different target materials.*

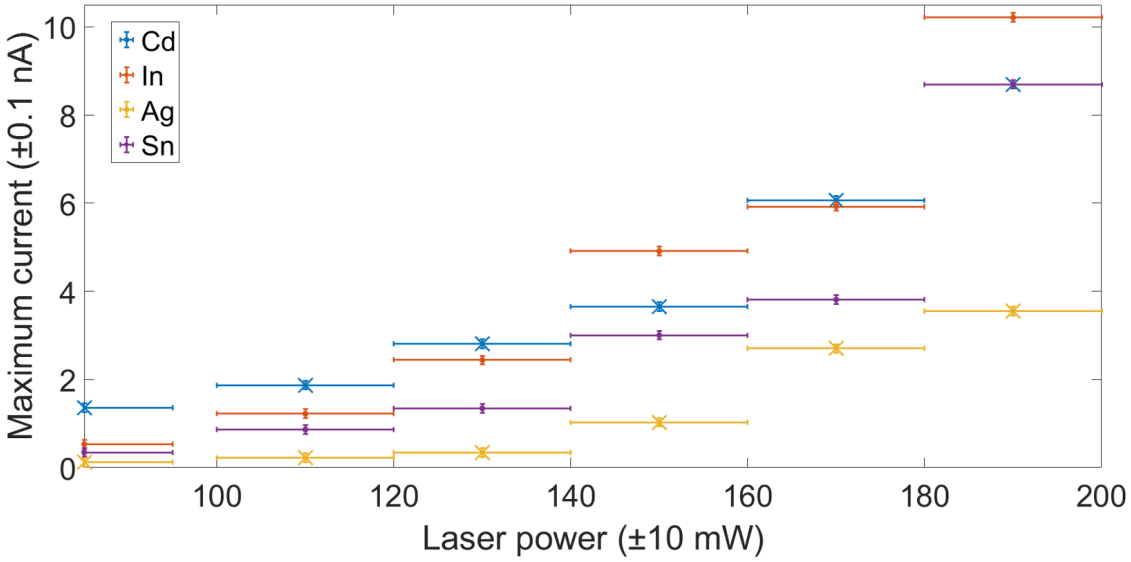

Figure 4.7: *Maximum current on the carpet measured during 5 minutes for the four different target materials.*

Table 4 gives an indication on how many particles are reaching the carpet on average for each target material between laser power 85 - 190 mW. For this, the currents from Figure 4.6 are converted to the amount of charges.

Table 4: *Number of charges on the carpet for different targets at lowest and highest laser power used for measurements in figure 4.6*

	Average number of charges per second on carpet ($*10^{10}$) ± 0.01	
Material	On 85 mW	On 190mW
Cadmium	0.58	4.52
Indium	0.037	1.82
Silver	0.017	1.42
Tin	0.036	1.35

4.2 Ion guide simulations

In order to optimize the efficiency of the ion guide, ion optical simulations are performed. These simulations will give insight in what values the different parameters of the ion guide should have in order to guide a maximum amount of ions through the ion guide.

4.2.1 Input of the simulation

For the simulations, the ion and electron optics simulator program SIMION [1] is used. The simulation includes the following:

- On scale model of the ion guide including hexapole 1, lens 1,2,3 and hexapole 2 with the aperture behind (see Figure 4.8.)

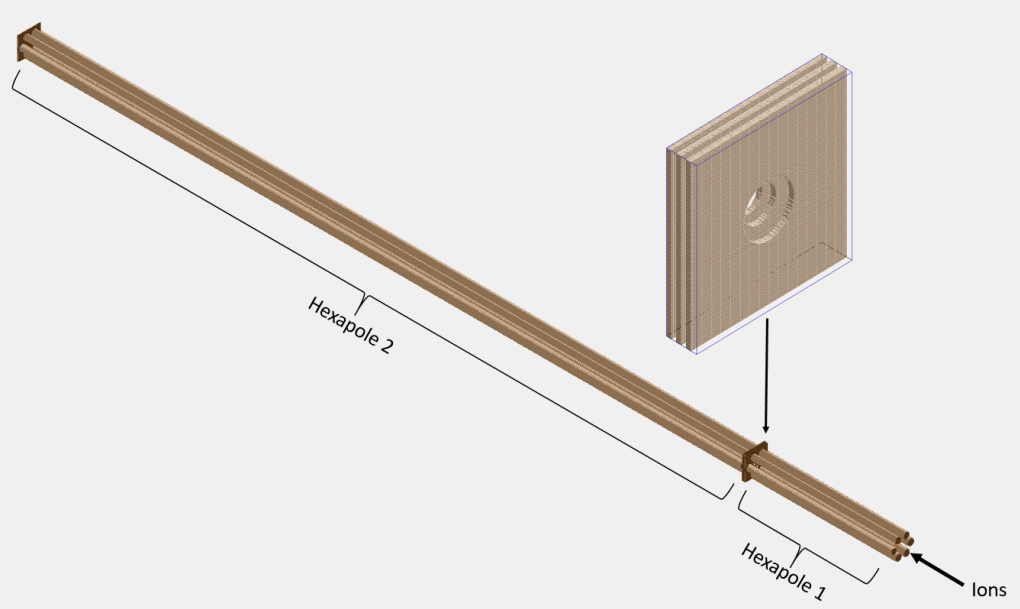

Figure 4.8: *Layout of the ion guide in the SIMION simulation. Shown are the two hexapoles with between them the three lenses with apertures in decreasing size. Behind hexapole 2, another aperture is present. The ions come in at the indicated place at hexapole 1.*

- Helium gas is present allowing the ions to collide with gas particles. Parameters of the gas that can be changed are the pressure, gas mass (4 u for helium), temperature and the collision cross section between the gas particles and the ions. In the real setup, hexapole 1 is in a separate pressure region than hexapole 2 causing hexapole 2 to be in a lower pressure environment. This pressure difference is not included in the simulation for the full layout of the ion guide. Instead, a different work bench is made for hexapole 2 and the aperture to provide a different pressure in that region.

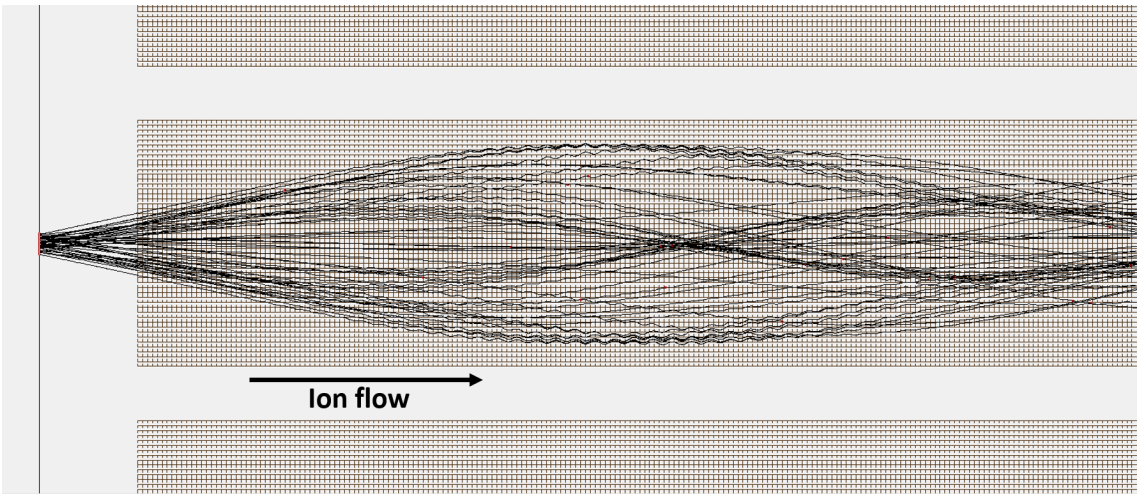

Figure 4.9: *Typical stable ion trajectories in the simulations. The ions come out of the carpet hole into hexapole 1 and stay confined in the hexapole.*

- Ions have a charge of +1 and initial kinetic energy of 2.8 eV due to the gas jet created by the carpet hole [15]. The ions are simulated into the ion guide like they are coming from the hole of the carpet. This means that the area in which the ions can spawn is a circle of the size of the carpet hole (0.45mm in diameter) of which the area is perpendicular to the direction of the hexapole rods. It is located at a distance of 2 mm in front of hexapole 1. The ions can fly out with a maximum angle of 13° with respect to the surface normal of the circle. When letting the ions fly into the separate work bench of hexapole 2, the circular area is equal to the area of the hole in lens 3 (3mm in diameter.) A typical simulation of ion trajectories is shown in Figure 4.9.

- Particle data are tracked and saved. Particle data include the starting point and end point of the ions, whether they cross the plane right behind the lenses and their kinetic energy.

- Both hexapoles include an RF voltage (U_{RF1} and U_{RF2} for hexapole 1 and hexapole 2 respectively.) This means that the voltage in the rods of the hexapoles will change from negative to positive with a certain frequency (f_{RF1} and f_{RF2},) leading the ions through the hexapole. The RF voltage will here be indicated as a peak to peak voltage (V_{p-p}.)

- The hexapoles and lenses have a DC offset voltage that will serve as an electric potential to the ions. These voltages will provide an electric potential gradient to the ions to get them smoothly through the ion guide.

According to the limitations of the real settings, the parameters provided in the simulation can be categorized as "adjustable," "fixed" or "unknown." This list is given in Table 5. A schematic of the ion guide with some parameter values and the DC gradient is shown in Figure 4.10.

Table 5: *Overview of parameters in the CISe setup*

Adjustable		**Fixed**		**Unknown**	
Parameter	***Value***	***Parameter***	***Value***	***Parameter***	***Remark***
p_{hex1}	$2 * 10^{-3}$ mbar	f_{RF1}	5.4 MHz	U_{RF1}	DC supply voltage
p_{hex2}	$5 * 10^{-5}$ mbar	f_{RF2}	2.5 MHz	U_{RF2}	
m_{ion}	stable isotopes	E_{kin}	2.8 eV [15]		
U_{DC1} and U_{lenses}	-15 – 15 V				
U_{DC2}	minimum -6 V				

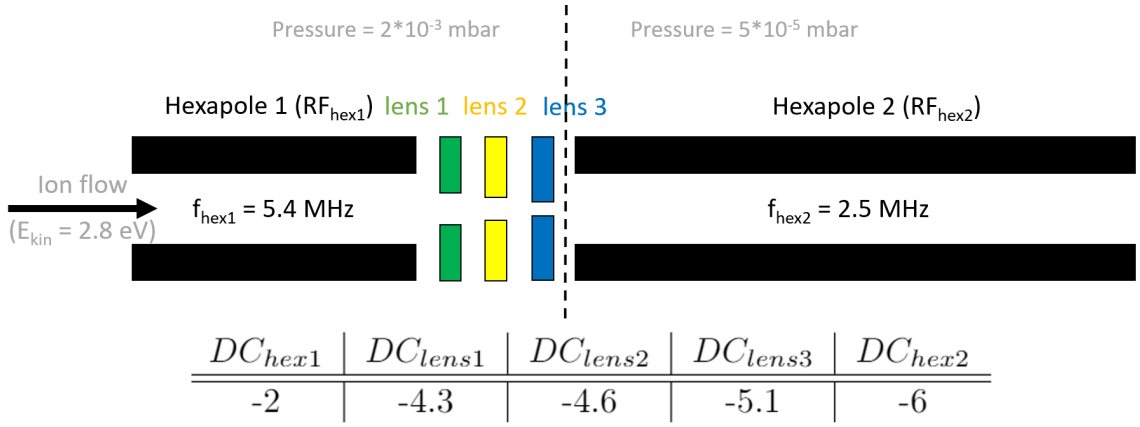

Figure 4.10: *Schematic of the ion guide (not on scale) with parameter values and the DC gradient.*

Some remarks on the parameters: The pressure around hexapole 1 can be adjusted by changing the pressure inside the gas catcher. However, this pressure should always be 50 mbar, since that is necessary for future experiments (see [15] and chapter 3.2.) Then, the pressure around hexapole 1 is $2 * 10^{-3}$mbar. It can thus be adjusted, keeping it at a fixed value is necessary.
Regarding the ions, four different materials are available (Cd, In, Ag, Sn) and their masses inside the setup are those of their stable isotopes. In the simulation, a mass range of 50 u - 600 u is chosen with a particle charge of +1. This is to account for doubly charged ions with mass 100 u (mass to charge ratio is then 100/2 u) and heavier charged molecules that can be present during the isobaric separation experiments.
U_{DC2} has a minimum value of -6V. With this in mind, the gradient given in Figure 4.10 can be used for the simulations in this thesis. For this gradient, the difference between the voltages of the lenses is very small. Some fluctuations in the DC voltages in the lenses will lead to a gradient that might not be suitable for guiding ions, since every consecutive lens should have a lower voltage than the previous one. To prevent this, a gradient where these differences are larger is needed. This needs to be investigated in future experiments.
The RF voltages of both hexapoles is unknown and their optimal values need to be established using these simulations. In the setup, U_{RF1} can be changed by adjusting the DC voltage that is supplying the RF voltage, but the RF voltage is not indicated. U_{RF2} is also not indicated

and is provided by the qToF on which it cannot be changed. The frequencies of hexapole 1 and hexapole 2 in the setup are measured to be respectively 5.4 MHz and 2.5 MHz. These frequencies are in disagreement with the specifications in the manuals. In there is written that the frequency should be 1 MHz.

4.2.2 Stability region

In order to optimize the ion transmission yield of the ion guide, the stability region of its hexapoles has to be found. The stability region is the range of settings of the parameters that will confine the ions in the central axis of the hexapole and hence not let them fly out of the hexapole from the side. This thesis defines the stability region as the RF voltage range on a certain DC offset on a certain frequency for a certain mass. A typical stability region is given in Figure 4.11. To find the stability region, the boundaries for the RF voltage (minimum RF and maximum RF) are obtained by simulating approximately 50 particles and determining whether the ions are confined in the hexapole or not.

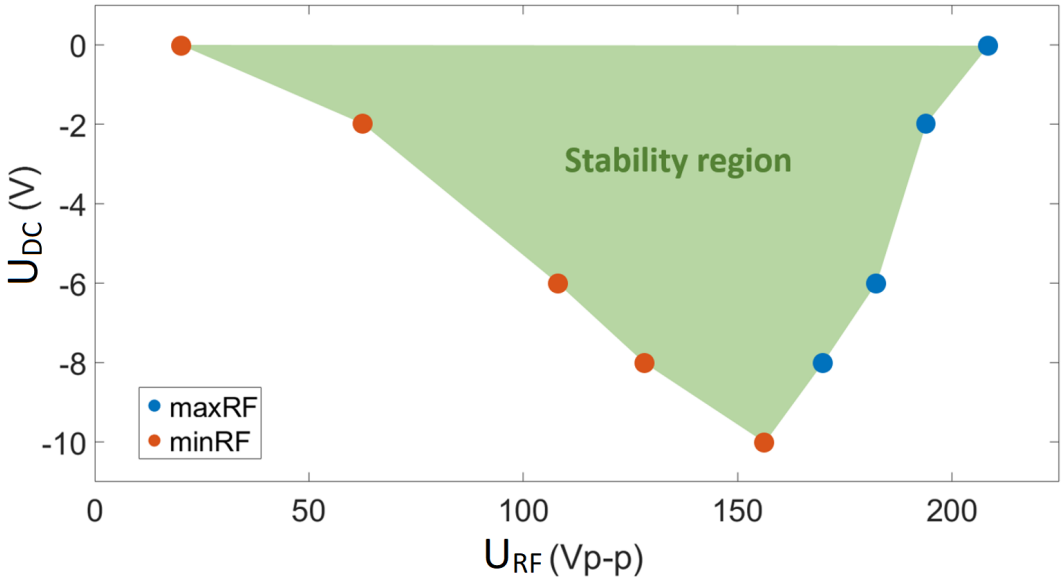

Figure 4.11: *Approximate stability region of a hexapole for ion m/z of 100 and a frequency of 1 MHz. The ion trajectories in the hexapole are stable for voltages within the green region. The same shape is also obtained for a positive DC offset.*

For an RF voltage outside this stability region, ions will not go through the hexapole. Figure 4.12 shows ion trajectories for an RF lower than the stability region and Figure 4.13 shows ion trajectories for an RF higher than the stability region. The boundary for the maximum RF is more continuous than the boundary for the minimum RF: for an RF that is too low, no ions will get through and for an RF that is too high, too many ions will get lost, but there are still some ions that will stay confined for long enough time to at least reach the end of the ion guide. Most of these ions are the ones that come in with a very small angle.

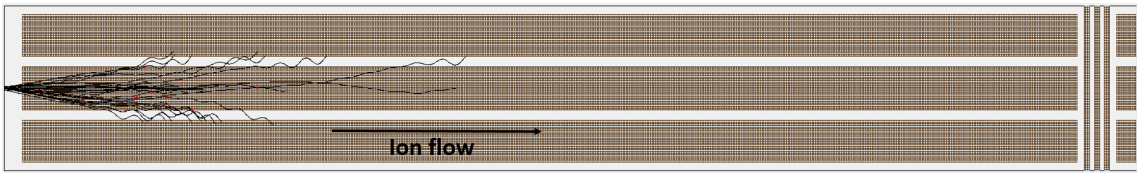

Figure 4.12: *Ion trajectories in the hexapole for an RF voltage that is a few volts lower than the boundary of the stability region. They will all fly out of the hexapole.*

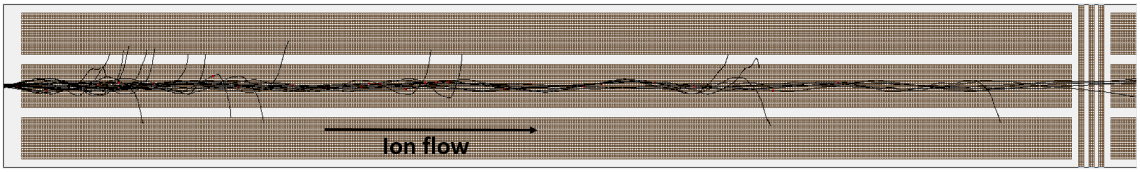

Figure 4.13: *Ion trajectories in the hexapole for an RF voltage that is a few volts higher than the boundary of the stability region. Some ions will get lost, some will stay in the hexapole.*

The determining for the stability region is done for the complete mass range of 50 u - 600 u and the single mass values of 50 u, 100 u, and 600 u on frequencies of 1 MHz and 2.5 MHz for singly charged ions. A frequency of 1 MHz is chosen, since this is a typical frequency for hexapoles and hexapole 1 in the setup will have this frequency if is decided to employ a new RF power supply for this hexapole. A frequency of 2.5 MHz is chosen to account for the frequency for hexapole 2. The results for the stable RF voltage ranges for these masses and frequencies are given in Tables 6 - 9. Note: the stability regions apply to both hexapole 1 and hexapole 2, since they have the same dimensions except for the length. The stability of a multipole does not depend on the length since the particle will experience the same electric field along the complete length of the hexapole [17]. Note: The stability does not depend on ion energy, pressure or collision cross section of the ions with the gas. These parameters might change the distance an ion can travel through the hexapole, but it does not change the stability. For example, for a higher pressure, an ion will get slowed down more easily, so it stops after a certain distance, but they will stay confined in the hexapole if it is in the stability region. The collision cross section used in the simulations is $\sigma = 4.2 * 10^{-19}$ m^2 which is the collision cross section for a tin ion with helium gas.

Table 6: *U_{RF} range for masses 50 u - 600 u. "no range" indicates that for this U_{DC}, there is no U_{RF} for which the particles for this mass stay confined in the hexapole.*

Mass range 50 u - 600 u		
Frequency (MHz)	**DC offset (V)**	**RF voltage rang (V_{p-p})**
1	0	26 - 106
	-2	no range
2	0	44 - 344
	-2	312 - 332
	-6	no range
2.5	0	124 - 652
	-2	360 - 632
	-6	no range

Table 7: *U_{RF} range for mass 50 u.*

Mass 50 u		
Frequency (MHz)	**DC offset (V)**	**RF voltage rang (V_{p-p})**
1	0	18 - 106
	-2	50 - 100
	-6	88
2.5	0	32 - 652
	-2	108 - 632
	-6	188 - 620

Table 8: *U_{RF} range for mass 100 u.*

Mass 100 u		
Frequency (MHz)	**DC offset (V)**	**RF voltage rang (V_{p-p})**
1	0	20 - 208
	-2	62 - 198
	-6	108 - 184
2.5	0	50 - 1300
	-2	154 - 1250
	-6	254 - 1240

Table 9: *U_{RF} range for mass 600 u.*

Mass 600 u		
Frequency (MHz)	**DC offset (V)**	**RF voltage rang (V_{p-p})**
1	0	26 - 1340
	-2	144 - 1336
	-6	252 - 1302
2.5	0	124 - >10000
	-2	360 - >10000
	-6	628 - >10000

4.2.3 Investigating yields

Using the stability region as a guideline, the yields of the ion extraction for both hexapoles are investigated. The aim was to find the optimal guidance for the mass range 50 u - 600 u, such that it results in the maximum transmission rate. For these simulations, approximately 1000 ions are simulated. The transmission yield for hexapole 1 is the percentage of these ions that go through hexapole 1 and all three of the lenses and therefore will reach hexapole 2. The initial energy is 2.8 eV, the pressure is $2*10^{-3}$ mbar and the DC gradient shown in Figure 4.10 is used. This means that U_{DC1} = -2 V. Table 6 shows that for a frequency of 2.5 MHz, the RF stability range for all masses between 50 u and 600 u is relatively large. An U_{RF1} within this range, say 500 V_{p-p}, is chosen and the ions are simulated into hexapole 1. The percentage of ions that will pass all three lenses is given as the yield. The results for different masses is given in Table 10. Trajectories of ions going through the lenses are shown in figure 4.14.

Table 10: *Yield for hexapole 1 on a frequency of 2.5 MHz for different masses.*

f_{hex1} = 2.5 MHz, RF_{hex1} = 500 V_{p-p}	
Mass (u)	**Yield (% of ions that cross the lenses)**
50	99.4%
100	99.5%
200	98.8%
600	83.3%

Since the typical frequency of an RF hexapole is 1 MHz, the transmission yield for hexapole 1 is also investigated for this frequency. This is done for four different RF voltages. The results are given in Tables 11 - 14. These results show that a lower RF voltage leads to a higher yield for low masses and a lower yield for high masses. On the other end, a higher RF voltage leads to a lower yield for low masses and a higher yield for high masses. This is also indicated by the stability range in Tables 7, 8 and 9. The yield for 100 u and 200 u ions will stay close to 100% for all the four investigated RF voltages. Hence, the hexapole can serve as a low mass- or high mass transmitter by adjusting U_{RF}.

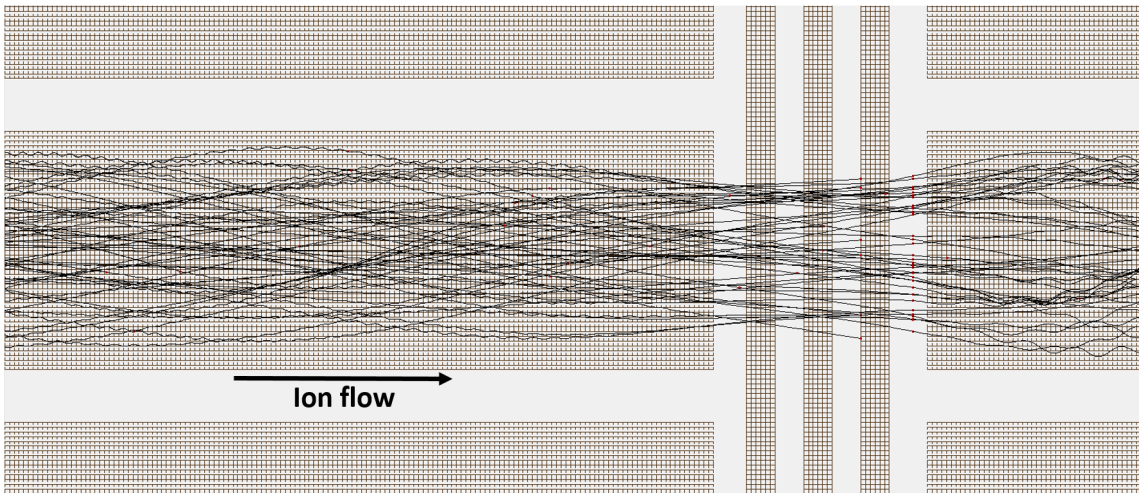

Figure 4.14: *Trajectories of ions that go through the three lenses after leaving hexapole 1.*

Table 11: *Ion transmission yield for hexapole 1 on* f_{RF1} *= 1 MHz and* $URF1$ *= 150* V_{p-p} *for different masses.*

f_{RF1} = 1 MHz, U_{RF1} = 150 V_{p-p}	
Mass (u)	**Yield (% of ions that cross the lenses)**
50	93.7%
100	98.9%
200	96.5%
600	65.9%

Table 12: *Ion transmission yield for hexapole 1 on* f_{RF1} *= 1 MHz and* U_{RF1} *= 170* V_{p-p} *for different masses.*

f_{RF1} = 1 MHz, U_{RF1} = 170 V_{p-p}	
Mass (u)	**Yield (% of ions that cross the lenses)**
50	91.5%
100	99.2%
200	98.1%
600	71.0%

Table 13: *Ion transmission yield for hexapole 1 on f_{RF1} = 1 MHz and U_{RF1} = 200 V_{p-p} for different masses.*

f_{RF1} = 1 MHz, U_{RF1} = 200 V_{p-p}	
Mass (u)	**Yield (% of ions that cross the lenses)**
50	82.4%
100	99.5%
200	98.4%
600	83.4%

Table 14: *Ion transmission yield for hexapole 1 on f_{RF1} = 1 MHz and U_{RF1} = 250 V_{p-p} for different masses.*

f_{RF1} = 1 MHz, U_{RF1} = 250 V_{p-p}	
Mass (u)	**Yield (% of ions that cross the lenses)**
50	58.5%
100	99.8%
200	99.3%
600	96.1%

In order to investigate the yield of hexapole 2, a separate work bench is used that only contains hexapole 2 and the aperture that is behind it. The pressure put into here is $5 * 10^{-5}$ mbar. The ions are injected into hexapole 2 as they are ejected from lens 3. They will spawn within a circle that is the size of lens 3 (diameter of 3 mm) with an angle of maximally 11°. The initial kinetic energy of the ions in this work bench is equal to the average energy the ions have after they leave lens 3 obtained in the simulations for hexapole 1 and is set on 6.6 eV. The investigated frequency is 2.5 MHz which is the measured frequency of hexapole 2. This frequency is set by the qToF and cannot be changed easily, so only this frequency is investigated.
U_{DC2} = -6 V to keep the gradient given in Figure 4.10. According to Table 6 there is no U_{RF2} in the stability region for all the masses between 50 u and 600 u for this U_{DC2}. Therefore, it is chosen to investigate two values of U_{RF2}. One outside the stability region of 600 u ions (500 V_{p-p}) and one outside the stability region for 50 u ions (720 V_{p-p}.) For these simulations, two types of yield can be defined: the percentage of ions that stay in the hexapole and reach the aperture and the percentage of ions that go through the aperture. Trajectories of ions that reach the aperture are shown in Figure 4.15.
The results for these simulations are given in Tables 15 and 16. The tables show that for the lower RF voltage, no ions of 600 u stay confined in the hexapole (see Table 15.) This is a logical observation, since this voltage is lower than the minimum U_{RF2} that the hexapole should have to confine these heavier ions. For the higher U_{RF2}, the ions with mass of 600 u are now all reaching the aperture (see Table 16.) The downside of this is that now the yield of mass 50 u ions to reach the aperture is not 100% anymore. A remarkable observation is that the percentage of them going through the aperture has not been reduced very much compared to that in Table 15. It can be concluded that U_{RF2} = 720 V_{p-p} is more efficient for the whole range of masses.

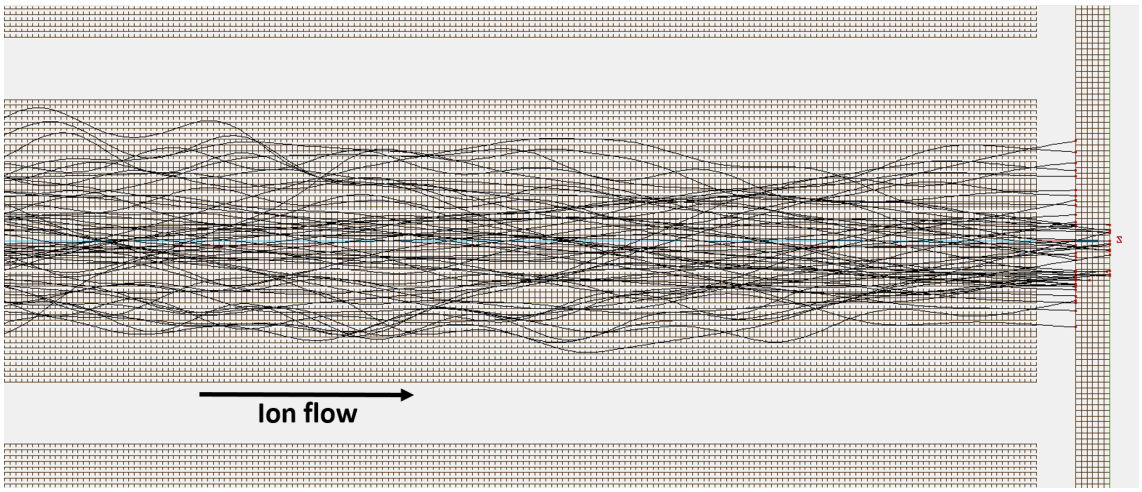

Figure 4.15: *Trajectories of ions that reach the aperture behind hexapole 2. Some will go through the aperture and some will hit the electrode.*

Also the yield for entering the aperture is quite low. This has to do with the fact that the aperture is quite small (1.1 mm in diameter.) There are no simulations done for a larger aperture, but expected is that this will improve the overall yield of the ion guide. The aperture connects with the next parts of the qToF. Changing its size may complicate the extraction of ions in the next parts of the qToF and the filter function of the quadrupole mass spectrometer.

Table 15: *Ion transmission yield for hexapole 2 on* f_{RF2} *= 2.5 MHz and* U_{RF2} *= 500* V_{p-p} *for different masses.*

f_{hex2} = 2.5 MHz, RF_{hex2} = 500 V_{p-p}		
Mass (u)	**Yield (% of ions that stay confined in hexapole 2)**	**Yield (% of ions that go through the aperture)**
50	100%	28.0%
100	100%	32.0%
200	100%	11.3%
600	0%	0%

Table 16: *Ion transmission yield for hexapole 2 on f_{RF2} = 2.5 MHz and U_{RF2} = 720 V_{p-p} for different masses.*

f_{hex2} = 2.5 MHz, RF_{hex2} = 720 V_{p-p}		
Mass (u)	**Yield (% of ions that stay confined in hexapole 2)**	**Yield (% of ions that go through the aperture)**
50	68.9%	26.3%
100	100%	30.8%
200	100%	13.7%
600	100%	19.8%

4.2.4 Lens 2 as a Faraday cup

A way to check if the carpet and hexapole 1 are working properly is to use lens 2 as a Faraday cup (number 5. in Figure 4.1.) Doing that, will indicate whether particles reach lens 2 and thus have gone through the carpet and hexapole 1. For this, the multimeter needs to be connected to one of the lenses. In order to do this, a box is made to separate the connections of the lenses from each other (see Figure 4.16.) The multimeter is then connected to lens 2 as shown in Figure 4.17.
The DC voltages that can be used for this experiment can be for example: U_{DC1} = -2 V, U_{lens1} = -2 V, U_{lens2} = -2 V, U_{lens3} = 5 V. U_{RF1} should be within the stability region for the given frequency. For these settings, around 70% of the ions will hit lens 2. The trajectories of the ions when they hit lens 2 can be seen in Figure 4.18. Using lens 2 as a Faraday cup will also be useful for tuning the carpet and hexapole 1. The optimal settings are reached for a maximal current received from lens 2.
Note: Figure 4.18 shows that some ions that hit lens 2 do that by flying back after passing lens 2. This may not work in the real setup, since the gas jet will also help pushing them in the direction of the qToF. The gas jet is not present in the simulation.

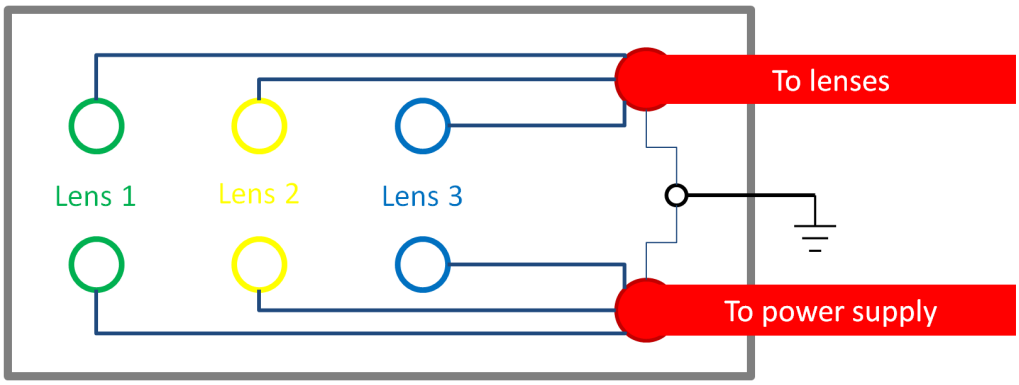

Figure 4.16: *Schematic of the connector box used to split the connections of the lenses in order to connect the multimeter to one of them.*

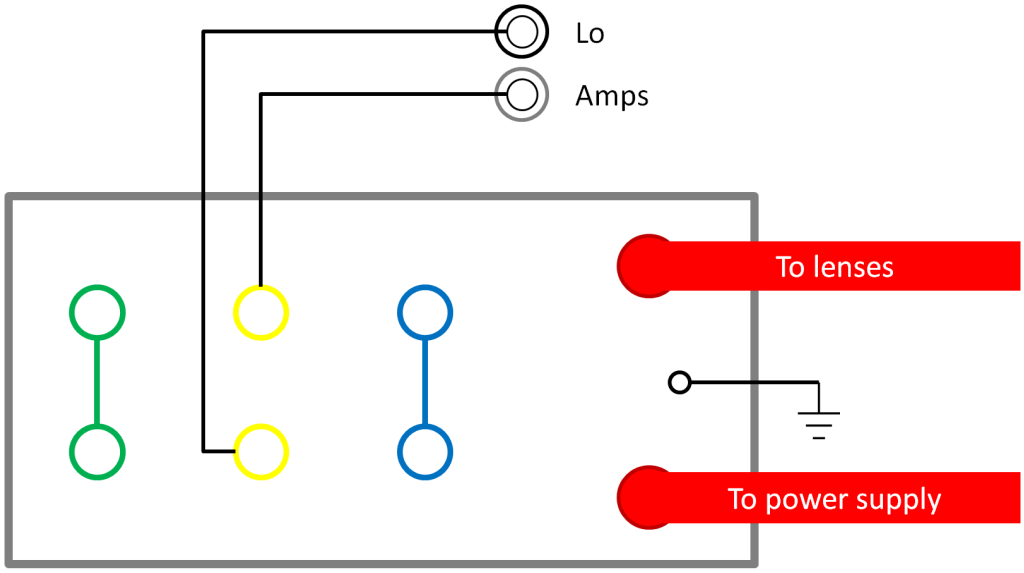

Figure 4.17: *Schematic of how the multimeter is connected to the connector box of the lenses to measure the current on lens 2.*

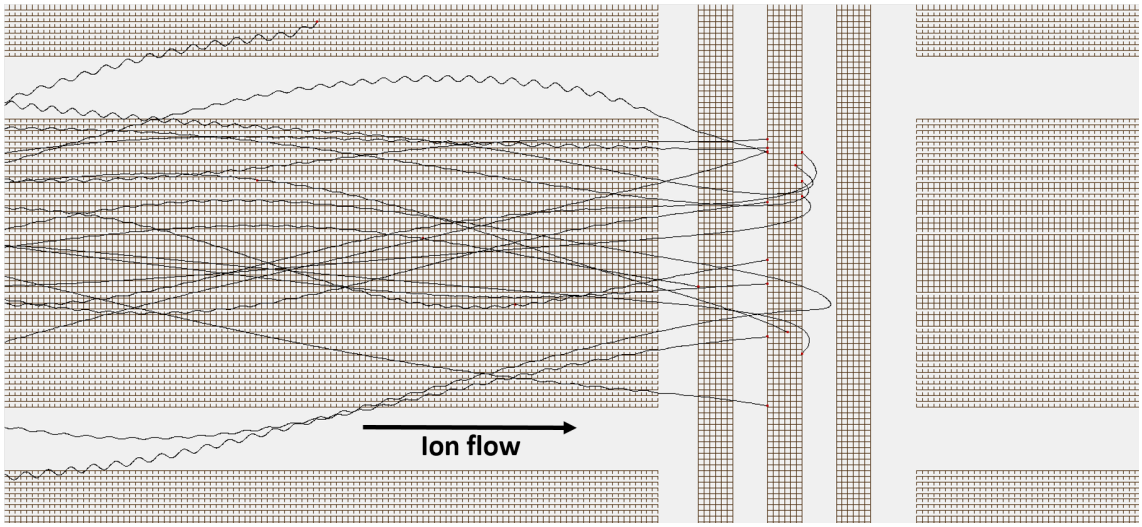

Figure 4.18: *Using lens 2 as a Faraday cup. Ion trajectories end on lens 2.*

5 Conclusion

This thesis shows some experiments on the transmission of ions created by laser ablation from a gas catcher. The creation of ions of the stable isotopes of Ag, In, Cd, and Sn is observed as the induced current in the target holder. It is concluded that silver has the highest ablation threshold because of its high melting point and large thermal conductivity. Cadmium has the most constant ablation rate while the other materials show a very large peak current compared to their average current. The amount of ions that hit the carpet, and are therefore available for extraction to the ion guide section, is investigated using the carpet as a Faraday cup. It is seen that the amount of ions on the carpet increases for a larger target holder voltage and electric field gradient. An optimal- or saturation voltage is not observed. Most current is detected at U_{cage} = 300 V. A number of charges ranging from 1.7*10^8 e to 4.5*10^{10} e has been observed.
The stability of the hexapoles in the ion guide has been explored and the transmission yields for the whole ion guide have been investigated using electro-optical simulations. The stability is presented as a range for the RF voltage and DC offset for a given RF frequency and ion mass to charge ratio for which the ions stay confined in the hexapole. This has been investigated for ions with a m/z range of 50 - 600. For f_{RF} = 1 MHz there is a U_{RF} range for where the trajectories of all the ions within the m/z range are stable if U_{DC} = 0 V, but not when U_{DC} = -2 V or larger. For f_{RF} = 2.5 MHz there is a U_{RF} stability range for a DC offset voltage of U_{DC} = -6 V. From this could be concluded that lowering the RF voltage increases the transmission yield for lighter particles and that increasing the RF voltage increases the transmission yield for heavier particles. This is confirmed by simulations of the transmission yields of ions going through the ion guide: setting f_{RF} = 1 MHz and U_{DC} = -2 V, the transmission yield through hexapole 1 is close to 100% for m/z values of 50 - 200 if U_{RF} = 150 V_{p-p} and for m/z values of 100 - 600 if U_{RF} = 250 V_{p-p}. Additionally, a method to observe particles inside the ion guide by using lens 2 in the ion guide as a Faraday cup is proposed. U_{lens3} needs to be around 5 V in order to repel the ions and let them hit lens 2. Detecting ions on lens 2 indicates that ions are guided by the carpet and hexapole 1.

In order to optimize the ion transmission of the setup further, more consistent measurements should be done on the guidance of the electrical gradient of the cage. For each series of measurements, the angle between the beam and the target needs to be consistent and each measurement needs to be done on a fresh spot on the target. This will give results that can be much better compared to each other. Doing simultaneous measurements on the current on the target holder and the carpet will give more insight in how these two currents are related and if the current measured on the target holder does indeed represent the amount of electrons removed from the target by laser ablation.
More research should also be done on the performance of the ion guide. The proposed method to use a lens as a Faraday cup can be used for the ion transmission from hexapole 1. The MCP detector in the qToF can be used to optimize the ion transmission through the whole setup once ions are systematically detected. If this is achieved, the performance of the carpet can be investigated and subsequently, the voltages in the ion guide should be tuned such that this results in the highest transmission rate possible. Experiments on chemical isobaric separation can only be executed when the ion transmission in the setup is fully optimized. Doing more simulations on the DC gradient of the ion guide and on the ion transmission yields for both hexapoles on different DC offsets can also help optimizing the transmission of the setup.

Acknowledgements

In this section I want to thank all the people that helped me through the time I was conducting this thesis. First of all, I want to thank my supervisor Prof. Dr. Julia Even for showing me the world of university research. I really appreciate the opportunities you gave me, in particular the participating in the beam time for SHIPTRAP at GSI.
Special thanks goes to Luisa for guiding me through the setup and the aim of the CISe project. It was very pleasant to work with you and to explore the functions and malfunctions of the setup together. I wish you good luck with continuing the project together with Ludovica.
I want to thank Mark too for helping us many times with problems in the setup regarding electrical connections. You did not only help us, but I also learned a lot from you about electricity.
Thanks also goes to the people working on the projects supervised by Julia and provided nice discussion points in the meetings on Fridays: Arif, XiangCheng, Brankica, Nathan, Ludovica, Lisa, Briain, Gawein, Maarten, Bara as well as the people in the FIS meetings on Thursday with special thank to my second supervisor Prof. Dr. Steven Hoekstra.
All in all, I can look back on a period with ups and downs, but the most important part was learning from the experiences I went through.

References

[1] Scientific Instrument Services. *SIMION version 2020*. URL: https://simion.com/.

[2] H. Schatz et al. "End Point of the rp Process on Accreting Neutron Stars". In: *Phys. rev. lett.* 86.16 (2001).

[3] G. Audi et al. "The AME2016 atomic mass evaluation (I). Evaluation of input data; and adjustment procedures". In: *The nubase 2016 of nuclear properties* 41.3 (2017).

[4] M. Chartier et al. "Mass Measurement of ^{100}Sn". In: *Phys. rev. lett.* 77.12 (1996), pp. 2400–2403.

[5] National Nuclear Data Center. *Nudat 2.8*. URL: https://www.nndc.bnl.gov/nudat2/.

[6] R. E. Russo. "Laser Ablation". In: *Applied Spectroscopy* 49.9 (1995).

[7] Laser Photonics. *Laser Cleaning Rust and Other Laser Ablation Applications*. URL: https://www.laserphotonics.com/laser-cleaning-rust-and-other-laser-ablation-applications.

[8] IPG Photonics. *Drilling*. URL: https://www.ipgphotonics.com/en/applications/materials-processing/drilling.

[9] All About Vision. *LASIK surgery: A brief guide*. 2021. URL: https://www.allaboutvision.com/visionsurgery/lasik.htm.

[10] D. Margarone L. Torrisi A. Borrielli. "Study on the ablation threshold induced by pulsed lasers at different wavelengths". In: *Nuclear Instruments and Methods in Physics Research B* 255 (2006), pp. 373–379.

[11] NIST Atomic Spectra Database. *Ionization Energies Data*. URL: https://physics.nist.gov/PhysRefData/ASD/ionEnergy.html.

[12] periodictable.com. *Melting Point of the elements*. URL: https://periodictable.com/Properties/A/MeltingPoint.an.html.

[13] periodictable.com. *Thermal Conductivity of the elements*. URL: https://periodictable.com/Properties/A/ThermalConductivity.html.

[14] Continuum. *Minilite operation manual*. 2014.

[15] A. Mollaebrahimi et. al. "A setup to develop novel Chemical Isobaric SEparation (CISE)". In: *Nuclear Instruments and Methods in Physics Research Section B: Beam Interactions with Materials and Atoms* 463 (2020), pp. 508–511.

[16] University of Bielefeld. *Electrostatic hexapole*. 2001. URL: https://www.physik.uni-bielefeld.de/mop/es/hexapol_en.html.

[17] C. Hägg and I. Szabo. "New ion-optical devices utilizing oscillatory electric fields. II. stability of ion motion in a two-dimensional hexapole field". In: *International Journal of Mass Spectrometry and Ion Processes* 73 (1986), pp. 237–275.

[18] P. B. O'Connor et al. "A High Voltage RF Oscillator for Driving Multipole Ion Guides". In: *Journal of the American Society for Mass Spectrometry* 13 (2002), pp. 1370–1375.

[19] TRACES Centre. *Quadrupoles: How do they work?* 2020. URL: https://www.utsc.utoronto.ca/~traceslab/PDFs/MassSpec_QuadsInfo.pdf.

[20] J. Krása et al. “Target current: a useful parameter for characterizing laser ablation”. In: *Laser and Particle Beams* 35 (2017), pp. 170–176.

[21] G. W. Tautfest K. L. Brown. “Faraday-Cup Monitors for High-Energy Electron Beams”. In: *The Review Of Scientific Instruments* 27.9 (1956), pp. 696–702.